UNIVERSITY OF WINDSOR

Faculty of Engineering

Department of Mechanical, Automotive and Materials Engineering

Capstone Design (06-92-400-59)

Summer Semester Capstone Progress Report – 2017

Experimental Sounding Rocket - IREC

UNIVERSITY OF WINDSOR

Faculty of Engineering

Department of Mechanical, Automotive and Materials Engineering

Capstone Design (06-92-400-59)

Summer Semester Capstone Progress Report – 2017

Experimental Sounding Rocket - IREC

Submitted on Friday, August 4th, 2017

Patrick Pomerleau-Perron: Student ID: 10380091

Anthony Gudisey: Student ID: 104052765

Dethprasit Oudomsouk; Student ID: 104009341

Liza-Anastasia DiCecco; Student ID: 103994499

Alexandra Rose; Student ID: 104056905

Samuel Randall; Student ID: 104320561

Shannon Bosilac; Student ID: 103813691

Michael Gyan; Student ID: 103938431

Jonathon Schreiber; Student ID: 103999304

SIGNATURE PAGE

Summer Semester Capstone Progress Report – 2017

Experimental Sounding Rocket - IREC

No action by any design team member contravened the provisions of the Code of Ethics and we hereby reaffirm that the work presented in this report is solely the effort of the team members and that any work of others that was used during the execution of the design project or is included in the report has been suitably acknowledged through the standard practice of citing references and stating appropriate acknowledgments.

Patrick Pomerleau-Perron: Student ID: 10380091; Signature: 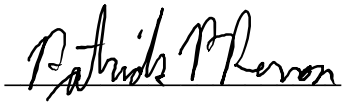 Date: 08/04/17

Anthony Gudisey: Student ID: 104052765; Signature: 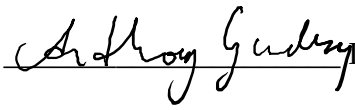 Date: 08/04/17

Dethprasit Oudomsouk; Student ID: 104009341; Signature: 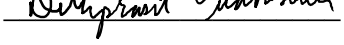 Date: 08/04/17

Liza-Anastasia DiCecco; Student ID: 103994499; Signature:  Date: 08/04/17

Alexandra Rose; Student ID: 104056905; Signature: 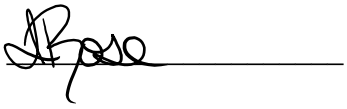 Date: 08/04/17

Samuel Randall; Student ID: 104320561; Signature:  Date: 08/04/17

Shannon Bosilac; Student ID: 103813691; Signature:  Date: 08/04/17

Michael Gyan; Student ID: 103938431; Signature:  Date: 08/04/17

Jonathon Schreiber; Student ID: 103999304; Signature: 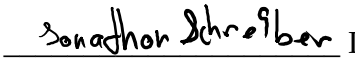 Date: 08/04/17

ABSTRACT

The objective of this project is to design and build a rocket that meets the design specifications for the 2017 Intercollegiate Rocket Engineering Competition (IREC) Spaceport America Cup (SAC) for the basic category of the competition. This involves building an experimental sounding rocket to carry a 8.8 lbs (4 kg) payload to an above ground level (AGL) peak altitude of 10,000 ft (3,048 m) using a commercial-off-the-shelf (COTS) solid or hybrid rocket propulsion system. Key features for the rocket in-question designed for the IREC by the University of Windsor Rocketry Team, *The Ambassador*, include an AeroTech M1845NT motor, a 6 inch (15.2 cm) diameter fiberglass tube, a 5.7-1 Von Kármán fiberglass nose cone, and three fiberglass 3/16 inch (0.476 cm) thick fins, with a total length of 96.5 inch (245 cm). *The Ambassador* implements a non-functional steel payload designed and manufactured in accordance with the CubeSat Standard. The major focus of the team is to create an accurate flight trajectory model, research and develop an aerodynamically optimized airframe structure, determine the optimal materials for the external and internal airframe components to ensure structural stability throughout flight, as well as explore the make of custom, in-house avionic solutions. Overall, *The Ambassador* successfully launched and was safely recovered at the 2017 IREC, reaching a peak AGL altitude of 3210 m. The University of Windsor Rocketry Team placed third in both the 10K COTS category and overall in the competition out of 82 rockets. This was obtained with an overall score of 814 out of a possible 1000 points based on the performance metrics of the competition. For future works, it is recommended that the next experimental sounding rocket capstone team explores the possibility of developing a functional payload as well as participate in a more advanced category of the competition.

NOMENCLATURE

a	=	cylinder diameter
A	=	amplitude of oscillation
A_{fp}	=	fin planform area
A_{fe}	=	fin exposed area
A_{ref}	=	cross sectional area of rocket body
A_i	=	acceleration component in i direction
C_p	=	pressure coefficient
C_{p1}	=	specific heat
C_{pT}	=	stagnation point pressure coefficient
$C_{D(i)}$	=	drag coefficient of component i
$C_{f(i)}$	=	coefficient of skin friction of component i
$C_{N\alpha(i)}$	=	stability derivative of component i
C_i'	=	compressibility corrected coefficient of drag of component i
C_x	=	force coefficient in the *x* direction
C_y	=	force coefficient in the *y* direction
d_b	=	diameter of rocket body
d_n	=	diameter of nose cone
d_d	=	diameter of tail
d_f	=	diameter at fin interference location
d_t	=	time step
f, g	=	generic functions
F_x	=	*X* component of the resultant pressure force acting on the vehicle
F_y	=	*Y* component of the resultant pressure force acting on the vehicle
g_0	=	gravitation acceleration
h	=	heat transfer coefficient
k	=	thermal conductivity coefficient
K	=	trailing-edge (TE) nondimensional angular deflection rate
K_{fb}	=	coefficient that takes into account an increase in normal force due to fin interference
l_m	=	fin median length
l_r	=	fin root chord length
l_t	=	fin tip chord length
l_s	=	height of fin
l_{TR}	=	length of rocket
l_n	=	length of nose cone
l_b	=	length of body tubing
l_c	=	length of tail
L	=	characteristic linear dimension
L_b	=	lapse rate
n	=	number of fins
Nu	=	Nusselt Number
M	=	molar ratio of air
M_a	=	Mach number
M_i	=	mass of component i
P	=	pressure
Pr	=	Prandtl Number
Re	=	Reynolds number

Re_{crit}	=	Critical Reynolds number
Rs	=	surface roughness
Ru	=	universal gas constant
T_b	=	sea level temperature
T_f	=	thickness of fin
V_i	=	velocity component in i direction
$X_{(i)}$	=	centre of mass location of component i
$X_{cm(i)}$	=	centre of mass location from nose tip of component i
$X_{cp(i)}$	=	centre of pressure location from nose tip of component i
X_f	=	fin leading edge distance from nose tip
δS	=	static stability
ρ	=	air density
μ	=	dynamic viscosity
γ	=	heat capacity of air

TABLE OF CONTENTS

SIGNATURE PAGE iii
ABSTRACT iv
NOMENCLATURE v
TABLE OF FIGURES viii
LIST OF TABLES ix
EXPERIMENTAL SOUNDING ROCKET - IREC 1
I. INTRODUCTION 1
II. DESIGN OBJECTIVES 1
III. STATE-OF-THE-ART 2
i. BODY TUBING 3
ii. NOSE CONE 3
iv. PREDICTION SOFTWARE 4
IV. DELIVERABLES 4
V. DESIGN METHODOLOGY, VALUES, & CONSTRAINTS 6
i. PROPULSION SUBSYSTEM 8
ii. AERO-STRUCTURE SUBSYSTEM 9
iii. RECOVERY SUBSYSTEM 12
iv. PAYLOAD SUBSYSTEM 15
VI. PHYSICAL IMPLEMENTATION 16
VII. EXPERIMENTAL RESULTS 18
i. AIRFRAME BODY TUBING TEST PROCEDURES AND RESULTS 18
ii. RECOVERY SYSTEM TESTING 20
iii. IREC 2017 COMPETITION RESULTS 21
VIII. DESIGN SPECIFICATIONS AND PERFORMANCE METRICS 22
IX. PROOF-OF-DESIGN-CONCEPT DEMONSTRATION 24
i. COMPUTATIONAL FLUID DYNAMICS ANALYSIS 24
ii. RESULT OVERVIEW 30
X. CONCLUSIONS & RECOMMENDATIONS 33
i. RECOMMENDATIONS 33
XI. ACKNOWLEDGEMENTS 34
REFERENCES 35
APPENDIX A: MISION CONCEPT OF OPERATIONS OF *THE AMBASSADOR* 37
APPENDIX B: HAZARD ANALYSIS APPENDIX 42
APPENDIX C: RISK ASSESSMENT APPENDIX 45
APPENDIX D: ASSEMBLY CHECKLIST 56
APPENDIX F: AVIONICS SELECTION ANALYSIS 65
APPENDIX G: ROCKET VEHICLE ANALYSIS 66
APPENDIX H: MATLAB TRAJECTORY MODEL 72

TABLE OF FIGURES

Figure 1: Cutaway Figure Depicting the Fully Integrated Launch Vehicle and its Major System Components 5
Figure 2: Design Process Flow Chart for The Ambassador 7
Figure 3: Descent Velocity vs Diameter of the Drogue Parachute 15
Figure 4: Descent Velocity vs Diameter of the Main Parachute 15
Figure 5: CubeSAT Standard [26] 16
Figure 6: Coefficient of Pressure: Nose Tip 27
Figure 7: Coefficient of Pressure: High Pressure Side 27
Figure 8: Coefficient of Pressure: Low Pressure Side 28
Figure 9: Isentropic Mach Number: Side View (High Pressure Side) 28
Figure 10: Isentropic Mach Number: Nose Tip 29
Figure 11: Isentropic Mach Number: Top Fin Side View (High Pressure Side) 29
Figure 12: Comparison of Altitude over Time between Dynamic Prediction Model and Eggtimer TRS 30
Figure 13: Comparison of Velocity over Time between Dynamic Prediction Model and Eggtimer TRS 31
Figure 14: Comparison of Flight Computer Altitudes over Time 31
Figure 15: Nominal phases of flight of The Ambassador 37
Figure 16: Wiring Diagram of the Arduino Avionics Component of The Ambassador 61
Figure 17: Custom Electronics - Wiring Diagram of the Eggtimer TRS and Quantum Avionics Solution of The Ambassador 61
Figure 18: Custom Electronics - Wiring Diagram of the Raspberry Pi Avionics Component 62
Figure 19: The Ambassador - Assembled CATIA Drawing 62
Figure 20: Motor Mount and Fin Assembly Drawing 63
Figure 21: Avionics Bay Overview Drawing 63
Figure 22: M1845NT-P Motor [3] 64

LIST OF TABLES

Table 1. Advantages and Disadvantages of High versus Low Burn Time Fuel Rates of Rocket Motors .. 8
Table 2. Result Summary of Three-Point Bend Testing 19
Table 3. Result Summary of Tensile Testing 19
Table 4: The Ambassador Report Flysheet Summary 22
Table 5: 2017 IREC Performance Scoring System 24
Table 6: CFD Mesh Specifications 25
Table 7: CFD Fluent Setup 25
Table 8: CFD Results 26
Table 9: Result Summary Comparison 32
Table 10: Result Summary Software Comparison 32
Table 11. Mission Concept of Operations Overview of The Ambassador 37
Table 12. Hazard Analysis Overview 42
Table 13. Risk Assessment Overview 45
Table 14. Avionics Cost Analysis 65

EXPERIMENTAL SOUNDING ROCKET - IREC

I. INTRODUCTION

This is the first year the University of Windsor has aimed to compete in the IREC. The deliverables of the capstone project involve the design and construction of an experimental sounding rocket following the rules and constraints set by the Experimental Sounding Rocket Association (ESRA) for the basic category of the 2017 IREC Spaceport America Cup. This involves building an experimental sounding rocket to carry a 4 kg payload to an above-ground-level (AGL) apogee of 3,048 m using a commercial-off-the-shelf solid propulsion system. The payload features a non-functional steel cube with tapped holes for weight adjustment to correspondingly adjust the apogee if necessary prior to the launch. A two-event recovery system, or dual-deployment system, is implemented to ensure safe landing of the rocket after reaching its peak altitude. The main body is separated at apogee using a black powder ejection charge inside the rocket to deploy a small parachute or drogue to maintain a controlled descent velocity between 23 m/s and 46 m/s from apogee to approximately 366 m AGL. At this altitude, a much larger parachute is then deploibyed using another black powder ejection charge at a different separation location along the rocket's body, to dramatically reduce the descent velocity to under 9 m/s to ensure safe ground landing.

The experimental sounding rocket capstone, being a relatively new project at the University of Windsor, involves research on vehicle design and optimization, material selection, predictive analysis, as well as avionics software programming and development, which are the focus of this year's team. With limited resources and experience, the major goal of the team involves building a solid foundation for future teams. This consists in understanding the physics behind rocket flight performance to create an accurate trajectory model in MATLAB. Existing software packages for predictive trajectory modelling that are commonly used are RockSIM and OpenRocket. These programs however, operate on a 'black box' interface in which background calculations are hidden from the user and are not thoroughly documented. The available software options also tend to significantly overshoot predicted apogees due to a lack of user control over specific input variables. More specifically, these software options do not accurately model transonic flight, restrict surface roughness height user input control, and omit contributions to the parasitic drag coefficient, such as protruding screw heads, vent holes, and body discontinuities, which have a combined effect on altitude performance. Hence, the development of an enhanced predictive dynamic model was deemed necessary to increase the user customizability, while improving the accuracy of the model than what is commercially available.

Other important project aspects include the research and development of an aerodynamically optimized airframe structure, determining the optimal materials for the external and internal airframe components to ensure structural stability throughout flight, as well as the exploration of the use of custom, in-house avionic solutions. Overall, key design factors that are analysed in vehicle design are the rocket geometry, weight, strength, and overall cost.

II. DESIGN OBJECTIVES

The main design objective of this capstone project involves the development of an experimental sounding rocket in accordance with the rules and constraints set by the ESRA for the

basic category of the 2017 IREC SAC. This would include designing and building an experimental sounding rocket to carry a 4 kg payload to an AGL peak altitude of 3,048 m using a COTS solid propulsion system, as previously mentioned, which would be safely recovered and would record specific flight information such as altitude and velocity. The critical design constraints are listed below. The rocket must:

- Carry no less than 4 kg of payload. The payload must follow either the CubeSat or PocketQube standard
- Have a target apogee of 3,048 m (10,000 feet) AGL
- Not exceed 40,960 N-s of installed total impulse on take-off
- Have the initial recovery deployment (drogue chute) reduce to a total descent velocity of 23-46 m/s
- Have the main recovery system deployment (large parachute) at an altitude no higher than 457 m (1,500 feet) AGL
- Have a terminal impact velocity less than 9 m/s
- Not contain any self arming/targeting software
- Have pressure relief holes with recommended diameters between 0.30 to 0.47 cm
- Have a launch elevation angle of 84°±1° (Official may reduce angle to 70° based on weather)
- Have a launch rail departure velocity of at least 30.5 m/s
- Be dynamically stable during flight. Specifically, the static margin or stability (the distance between the centre of mass and centre of pressure) must be greater than one body diameter but should not greatly exceed two body diameters
- Have a radio beacon or similar transmitter, such as a Global Positioning System (GPS), for locating launch vehicles during recovery which shall be carried by each independently landed piece
- Carry a COTS barometric pressure altimeter with data storage capability for reporting the actual apogee after recovery
- Be able to accept the control box provided by ESRA (12V, 15A) [1], [2]
- Have redundant electronics.

As previously mentioned, another design objective involves the development of a dynamic prediction trajectory model, improving upon commonly used commercially available software such as OpenRocket and RockSIM. These trajectory models also tend to undershoot the drag coefficient profile with respect to Mach number, which is suspected to be one of the sources of error in apogee prediction compared to actual flight data. Thus, breaking down each component of the total drag coefficient and determining contributors to the drag coefficient that are neglected by OpenRocket and RockSIM are important starting points. Finally, atmospheric conditions such as pressure, temperature, and lapse rate must accurately match the launch site conditions at the competition location in New Mexico. In parallel, the team aimed to improve the user experience by enhancing the customizability of the trajectory model.

III. STATE-OF-THE-ART

Rocketry is an area of engineering where numerous factors need to be carefully considered during the design phase. Understanding these factors is critical for competent decision making. Learning the rationale also means that future designs can be improved by understanding causes of

previous design failures. The areas where research needs to be conducted about pre-existing designs or approaches include the rocket airframe, nosecone, fins, parachutes and prediction software.

i. BODY TUBING

The most basic component of the rocket is the body tubing, or the airframe. The most commonly used materials in high-power rockets include carbon fibre, fiberglass-wrapped phenolic tubing, and fiberglass. Each material comes with its own set of advantages and disadvantages. Starting with carbon fibre, the main advantage of using carbon fibre in an airframe is that it is light and strong, which in turn allows a selection of a lower-impulse and less costly motor. The main disadvantages are that carbon fibre is very expensive and that it causes interference with the frequency used for telemetry for on board GPS systems. The second option is fiberglass-wrapped phenolic tubing. The main advantages of this are that it is lightweight, but still strong. The downside of using this material is that it is structurally unstable at speeds that approach the transonic regime. The last material that is used frequently is fiberglass. Fiberglass is a strong material, can withstand the forces that it is subject to at transonic speeds, and is also cheaper than a carbon fibre body. The biggest disadvantage of this material lies in the fact that it is relatively heavy, and requires a higher-impulse motor to reach the same altitude.

Many pre-existing rocket designs vary in height and there are a few reasons for this. Taller rockets usually tend to carry more components on-board. A taller rocket means that the mass within the rocket can be more evenly distributed as there is a lot of free space. Second, a taller rocket is more prone to failing. The reason for this is that as a rocket enters the transonic regime during flight, there is a rapid increase in stresses across the body, and large bending moments are created from choosing a slender rocket design. These large bending moments increase the chances of bending or folding the rocket midflight, causing a catastrophic failure.

Rockets can also be short and compact. This leads to a rocket being lighter, but if it is too short, static stability may be an issue. There have been unstable competition rockets that have spiralled out of control, only to crash right into the ground and endangered people. A preferred range of ratios relating the length of the rocket to the diameter must be maintained for the vehicle to successfully reach apogee while remaining structurally intact and stable. This ratio is known as the slenderness ratio.

ii. NOSE CONE

The selection of an appropriate nosecone is a crucial part of a rocket design. The materials that are commonly used for the nosecone mirror those used for the body tubing, the main point of interest in the nose cone design lies in the shape of the nose. The shape of the nosecone determines its aerodynamic properties. Commonly used nosecone shapes include conical, ogive, LV Haack, Von Karman, Parabola and Power Series. Each of these shapes performs differently at different speeds. For instance, the Von Karman shape performs extremely well at transonic speeds, whereas the conical nosecone shape has a much more inferior performance at these same speeds. Based on the predicted speeds that the rocket reaches, an appropriate nosecone needs to be selected.

iii. FINS

The main purpose of fins is to provide stability to the rocket during flight. Due to this reason, the fins must first and foremost be structurally stable and secondly, they must be aerodynamically adequate. The first requirement can be broken down into two different categories. The first category deals with the material used, and the second deals with the approach used when attaching the fins to the rocket body. Commonly used fin materials include carbon fibre and fiberglass. The method of attachment is next considered. The most common and sturdy method is a through-the-wall attachment, this means that the fins slide into slits in the rocket body and are epoxied into place at each point of contact. The second point is the shape of the fins. For transonic ranges, the shape that provides the best performance is a trapezoidal fin. A bad fin design or attachment can result in a rocket flying off-course or crash into the ground right after liftoff.

iv. PREDICTION SOFTWARE

Upon successfully choosing all the materials required and designing the rocket, it is important to be able to predict how the rocket will behave during each flight phase. RockSIM and OpenRocket are two well-known prediction software that are generally used by teams entering the IREC. Each of these prediction software come with their own sets of strengths and flaws. RockSIM is a reliable software that is used for apogee predictions and is a great tool to find the stability of a rocket. The problem with RockSIM is that its predicted apogee is usually vastly higher than the actual result, it tends to overshoot the apogee by around 20%. OpenRocket is a software that is more accurate than RockSIM in apogee prediction, and produces an estimated overshoot error of around 10% on average. The problem with OpenRocket is that the stability that it provides for the rocket is not always accurate for more complex designs.

IV. DELIVERABLES

The Ambassador has four major subsystems: propulsion, aero-structure, recovery, and payload. A cutaway figure depicting the fully integrated launch vehicle and the major components of its subsystems, configured for the mission being flown in competition, is shown in Fig. 1. Each subsystem reflects the technical analyses used to support the design and manufacturing decisions made throughout the progress of this project, as highlighted in the *Design Methodology, Values, & Constraints* section of this report.

In the final design of *The Ambassador,* the aero-structure is primarily made from filament wound fiberglass, with the fins being made from G10 fiberglass. A filament wound fiberglass 5.7-1 Von Kármán nose cone with a metal reinforced tip supplied by Wildman Rocketry is selected for use in *The Ambassador*. The payload bay is featured inside the nose cone and is designed based on the CubeSat standard, which features a 10 cm by 10 cm by 10 cm steel block as a non-functional payload with tapped holes for weight adjustment to correspondingly adjust the apogee if necessary prior to the launch. For loading onto the launch rails, the rail buttons chosen for the final design rocket are three plastic airfoiled rail buttons from Apogee Components.

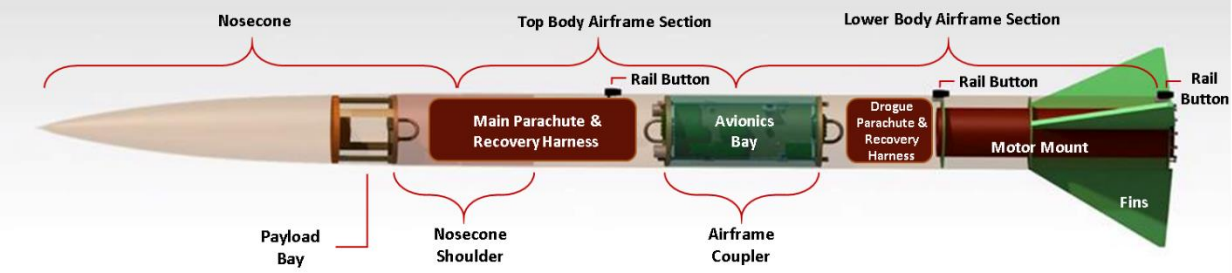

Figure 1: Cutaway Figure Depicting the Fully Integrated Launch Vehicle and its Major System Components

The propulsion subsystem of *The Ambassador* consists of the motor and the hardware set. The selected motor is an Aerotech M1845 which is held within the rocket using an RMS 98/7680 hardware set from Aerotech and is retained by a 98 mm flanged retainer ring. The hardware is seen in detail in Figure 21 of the Engineering Drawings appendix.

The recovery subsystem can be broken down into three main subsystems which are the avionics, the parachute and drogue and the recovery harness and linking mechanism. The avionics contain the altimeters and the black powder charges, and overall it controls the timing of the deployment of the parachute and the drogue. The Eggtimer TRS with a backup Eggtimer Quantum are selected for use in *The Ambassador*. The second recovery subsystem encompasses the parachute and the drogue. The recovery parachutes need to be accurately sized and selected so that the descent velocity will be within desirable bounds and they must also be strong enough to sustain the shock forces caused by opening. To meet these requirements, the drogue parachute is selected from Spherachutes as a 48 in (1.22 m) parachute while the main parachute is a SkyAngle parachute of 109 in (2.76 m) size. The last part of the recovery subsystem is the recovery harness. The recovery harness must be chosen with care as it determines the strength and the efficiency of the attachment between the rocket body and the parachute. U-bolts are selected in design to link the recovery harness to the rocket body, coupler, and nose cone interfaces, for its superior stress distribution characteristics in comparison to eyebolts. U-bolts made from 304 stainless steel are selected for usage with inner diameters of 1 in (2.54 cm) and 1.5 in (3.81 cm) which are statically rated up to 435 lb (1935 N) and 610 lb (2713.4 N), respectively [3]. The recovery harness used in each separation event is four times the length of the rocket, 9.6 m, and is made of tubular nylon.

The avionics bay (Figure 22) is composed of a wooden sled, which is attached to two steel threaded rods which run the length of the bay. The sled is attached to the threaded rods by metal P-clamps which are covered in rubber. This dampens any possible vibrations. Allthreads are fastened to two fiberglass bulkheads which house the charge wells. The avionics are fastened to the sled by metal bolts which have been threaded into the wood, with additional nuts to ensure a solid connection. In compliance with the critical safety guidelines, 22AWG stranded wire is used throughout the avionics bay with the exception of the igniters and the batteries. Three rotary switches are used between the batteries and the flight computers to ensure that the flight computers are entirely unpowered prior to arming.

The prototype dynamic trajectory model is developed using MATLAB to validate the design of *The Ambassador* while accurately predicting its apogee. The model is initially created

considering only the bare minimum free-body-force diagrams of a high-power rocket including the basic forces. Developed from this is a more complex model, which includes additions such as the subcomponents of the drag force. Notably, the model considers skin drag due to a measured average surface roughness and parasitic drag due to protrusions in the vehicle body. A measure of stability is added to the model from this, where stability is a measure of how much the rocket can correct itself as it ascends to maximum altitude. An atmospheric model is added to the code as well which considers the launch site conditions, considering temperature and pressure variation with altitude.

V. DESIGN METHODOLOGY, VALUES, & CONSTRAINTS

Approaching the design of *The Ambassador*, many factors had to be taken into consideration to finalise the specifications of each subsystem component. Figure 2 overviews a process flow chart which highlights the main steps in the design methodology, which is followed by subsections overviewing the design and related values and constraints for each of the main subsystems.

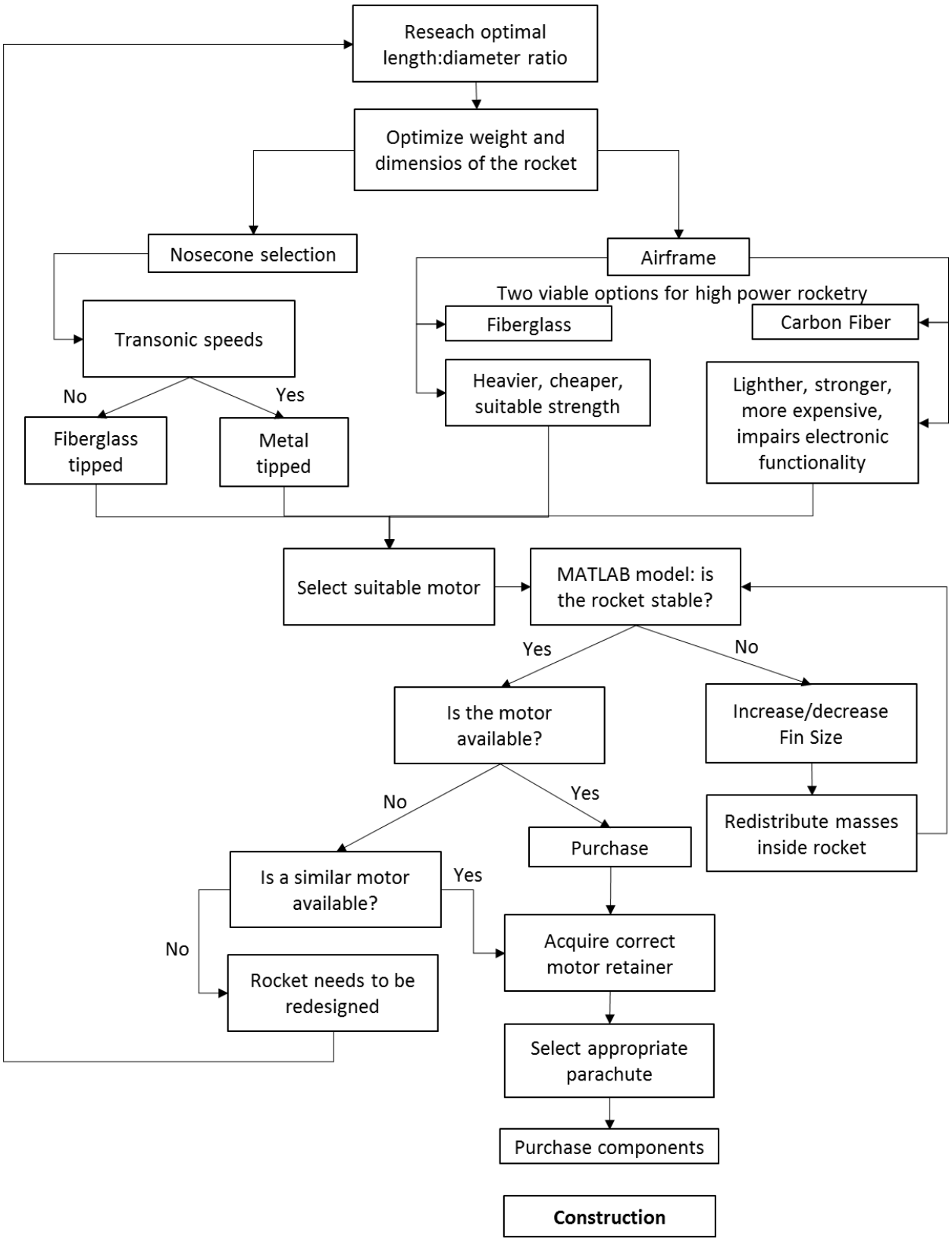

Figure 2: Design Process Flow Chart for The Ambassador

i. PROPULSION SUBSYSTEM

The design factors for selecting the rocket motor are the burn time, total impulse, rocket acceleration, and Mach number reached. The process is iterative because of the dependent nature of all the flight variables. The design of the rocket can be adjusted for each motor, signifying that the selection of two very different motors can lead to the same target apogee. Whereas one motor may be preferable, motor characteristics such as weight and burn time, will be important factors in determining whether a motor is viable or not. The best solution is determined on based on competition rules, cost analysis and the consideration of other related design constraints.

Three main characteristics analyzed for motor selection are burn time, average impulse over burn time, and motor weight. Burn time and average impulse are two related variables which dictate the acceleration of the rocket through powered flight. Burn time is the amount of time the motor will be burning and providing thrust, whereas the impulse is the amount of thrust produced over the burn time. These two factors result in a change in linear momentum of the rocket and thus a change in velocity. Therefore, based on this relationship, if a force is applied over a longer period, it will produce a larger deviation than the same force being applied briefly.

This idea is further expanded upon when considering the initial thrust. Consider two rockets that have two separate motors with the same impulse but differing burn times. The rocket with a higher burn time will experience a lower initial thrust leaving the guide rail. Throughout flight, a higher burn time also results in a slower flight velocity through powered flight. In contrast, a smaller burn time will result in the rocket travelling at faster speeds. There are many advantages and disadvantages to be considered when analyzing both situations, as presented in the following table.

Table 1. Advantages and Disadvantages of High versus Low Burn Time Fuel Rates of Rocket Motors

	Advantages	**Disadvantages**
High Burn Time	- Rocket is travelling slower and as a result, experiences lower body forces - More efficient, less drag	- Rocket takes longer to reach apogee - A slower rocket is more likely to be unstable during ascent
Low Burn Time	- Rocket achieves off the rail velocity required by competition rules - Rocket reaches apogee quicker - A quicker rocket is more likely to be stable during ascent - Higher drag	- Rocket moves faster and goes into transonic flow regime (close to Mach 1) which leads to large body forces and extreme stresses - This could also cause large shocks across rocket body and unexpected behaviour when compressibility must be considered

The availability of rocket motors is a factor that plays a major role in the motor selection. The first rocket design called for a 5 grain 75 mm motor from Cesaroni. This design was altered due to a mismatch in the weight of vehicle nose cone, which weighed more than anticipated. Due to the unavailability of a 75 mm motor with the required impulse for the new rocket weight, a new design

was required. This design requires the rocket to be shorter, the same idea goes for the rocket motor. The rocket motor chosen for the final design is the Aerotech M1845. It is 98 mm in diameter and 597 mm in length. It features a total impulse of 8307 N-s, along with a burn time of 4.4 seconds. The average thrust that the motor produces is 1845 N, whereas the maximum thrust is 3081 N. The hardware set that is used is the RMS-98/7680.

Subsection 8.2 of the Design, Test, & Evaluation Guide for the 2017 IREC states that the minimum off the rail velocity must be 30.5 m/s to ensure a stable and safe ascent. This is so that the rocket remains stable once it leaves the launch rail [1]. The motor chosen for The Ambassador powers the rocket to an end of rail velocity of 29.4 m/s, which is below the constraints specified by the rules. Within the same section of the rules, it is also stated that, "Alternatively, the team may prove stability is achieved at a lower rail departure velocity either theoretically (e.g. computer simulation) or empirically (e.g. flight testing) [1]". To this end, RockSIM, OpenRocket and MATLAB simulations confirmed that the rocket is stable at 29.4 m/s and a test launch of *The Ambassador* prior to competition proved that the rocket is stable during flight.

ii. AERO-STRUCTURE SUBSYSTEM

1. AIFRAME

Choosing a proper length for the body tubing entails finding the optimal slenderness ratio, which is the ratio of the total length of the rocket to the body diameter, as well as determining the necessary space allocation for the internal components the rocket. Research showed that the ratios that are commonly used which minimize drag ranged between 10:1 and 20:1. Due to the standard shape used for the payload bay, a minimum inner body tubing diameter is 5.5 in (13.97 cm) [4]. Therefore, the minimum diameter that could be used is 6.2 in (15.70 cm). With this information, maximum and minimum acceptable lengths are chosen considering the recommended slenderness ratio ranges. A final body tubing length is chosen by calculating the minimum required spacing of all the components such as the payload bay, coupler, parachutes, and motor mount.

The material selection of the body tubing is based on material testing and high-power rocket flight observations. Three types of tubing materials are tested which include: phenolic tubing, quantum tubing, and fiberglass wrapped phenolic tubing. Testing procedures and results from testing are summarized in the Experimental Testing section. Fiberglass wrapped phenolic tubing is observed to have the highest maximum tensile and bending strength, though with relatively high standard deviations. Of the three materials, the quantum tubing has the highest average bending strength, but lacks tensile strength. The phenolic tubing demonstrates inferior bending strength and tensile strength. Carbon fibre is eliminated as an option as it inhibits the radio frequency signal required by the avionics and is significantly more expensive. This process refined the selection to either fiberglass wrapped phenolic tubing or fiberglass tubing.

Based on the material tests, the tensile strength and flexural strength of the fiberglass wrapped phenolic tubing is 66.74 MPa and 4.33 MPa respectively. Due to the curvature of the tested samples, strength losses are stipulated to have occurred. The tensile strength of G-10 fiberglass based on fibre alignment is 262 MPa crosswise and 310 MPa lengthwise whereas the flexural strength of G-10 fiberglass is 448 MPa crosswise and 517 MPa lengthwise [5]. In high powered rocket flight observations, the body tube may experience an impact load comparable to the bend

test as the rocket landed. High power rockets that used fiberglass or carbon fibre tubing did not fracture due to impact or flight. In contrast, a score was produced during landing in the rocket using a phenolic tubing. Taking into consideration losses in tested samples, the G-10 fiberglass is determined to have superior mechanical properties at a similar cost and density than the fiberglass wrapped phenolic tubing and is thus selected as the airframe material. Carbon fibre is eliminated as an option because it hinders the functionality of the electronics.

2. NOSE CONE

Nose cone selection is essential in rocket airframe design. Design optimization for the nose cone and manufacturer selection are the main elements to this subcomponent. For high-power rockets flying at transonic 0.8-1.0 Mach range, optimal geometrical nose cone shapes that are recommended for superior aerodynamic properties include: LV-Haack, Von Kármán, Parabola, and x½ [6]. A fineness ratio (the ratio of the total nose cone length to the base diameter) of 5 is selected as NACA supersonic wind tunnel tests have proven this ratio to yield the lowest total drag (wave, friction, and form drag) [7].

Lack of manufacturing means and proper ventilation for fiberglass work at the University of Windsor workshop restricts the capabilities of the team to produce custom-made nose cone. Therefore, due to budgetary and timeline constraints that would be pressed if nose cone fabrication were to be outsourced, a design decision was made to eliminate this option and to analyze the market availability of 6 in (15.64 cm) diameter high power nose cones. Thorough research on market availability of high power nose cones based on a 6 in (15.64 cm) diameter was a high impact limiting design factor. Out of the four desired optimal geometrical shapes, only the Von Kármán shape is determined to be readily available for purchase. Market availability played a role in limiting material selection, as 6-in (15.64 cm) Von Kármán nose cones suitable for high power rocketry are found only available in fiberglass and carbon fibre. Carbon fibre is noted to inhibit some functionality features of the selected avionics in future reusability cases, eliminating it as a material option for the nose cone of *The Ambassador*. Thus, a fiberglass 5.7-1 Von Kármán nose cone supplied by Wildman Rocketry is selected for use in *The Ambassador*.

3. FINS

The fins serve to stabilize the rocket statically and dynamically. It is important to note that the presence of fins will increase interference and skin friction drag. Hence, in the calculations involved, there is a clear trade-off between maximizing stability and minimizing drag. The final fin dimensions are determined primarily in reference to NACA wind tunnel test results[8]–[10], theoretical aeroelastic results[11], and general fin optimization guidelines [7]. The number of fins, aspect ratio, sweep angle, semi span length, root chord, tip chord, leading edge, and trailing edge curvatures are investigated. For maximum altitude performance, three fins are used [8], each fin semi-span is one body diameter length, and the root chord is two body diameters in length to prevent flutter [9]. For the leading edge sweep angle when in transonic flight, NACA recommends the sweep angle to lie between 45 and 70 degrees from the cross-section of the rocket [10]. From the chosen root and tip chord lengths, this results in a sweep angle of 63.4° from the perpendicular of the rocket. The clipped delta shape with square edges also lowers the roll rate and the presence of fin tip vortices [7]. Finally, the trailing edge of each fin is slanted slightly forward to reduce the chances of clipping the fins when landing on the ground after recovery.

For the fins selected, flutter analysis is performed using Rocket Science and Technology's FLUTTER MARGIN1 Excel sheet [12]. Fin flutter is a function of the normalized thickness, taper and aspect ratios, and free stream pressure and speed of sound. The values for both speed of sound and altitude vary with time [13], thus a model is developed using pressure versus altitude as well as speed of sound vs altitude distribution charts. At maximum Mach number (0.81), FLUTTER MARGIN1calculates a margin of safety of approximately 7.5 [12]. The trajectory calculations done on the final rocket design in RockSim, OpenRocket, and the developed predictive MATLAB code results in top speeds ranging approximately from Mach 0.7 to 0.9, therefore, flutter will not be a problem. Three 3/16-inch-thick fins were also selected over 1/8-inch-thick for a more solid contact to the fiberglass motor mount. No reinforcing blocks need to be epoxied to the motor mount to reinforce the fins due to their adequate thickness.

The final dimensions to be determined are the leading edge and trailing edge chamfers. The leading edge is tapered and rounded slightly, and the trailing edges are tapered and blunt. The reason for this hybrid shape is to handle both transonic flow and subsonic flow, a combination of what is recommended by NACA [10] and what the team advisor recommended. Though these chosen shapes only minimally contribute to an increase in altitude, the purpose of attributing this hybrid shape is to prevent localized shock waves that square edged fins may cause due to a sharp increase in pressure. This is somewhat validated after conducting a steady 3D simulation in ANSYS Fluent 17.0, detailed in the Computational Fluid Dynamics subsection, showing that there are no shockwaves propagating along the length of either fin in the "worst case" scenario at maximum Mach number (0.81) and at a high angle of attack of 5°.

The fins need to be structurally stable to ensure safe and direct flight paths. The design involves a standard through-the-wall installation of the fins epoxied onto the motor mount fiberglass and in between the airframe slits. The fins are wedged between two centering rings and secured with epoxy to the surfaces of the rings. The fin can is reinforced with allthreads equipped with a thrust ring at the base of the rocket. The advantage of this design over others is the structural stability that it withstands.

4. RAIL BUTTONS

Rail buttons are used on a rocket to keep the body attached and sliding along the launch guide rail to ensure that the rocket is aimed and maintains its course during the initial acceleration at liftoff. The rail buttons are affixed to the exterior surface of the rocket along its length, one near the trailing end and one near its centre of mass. Commercially available rail buttons are generally made from some type plastic like nylon or delrin. In a report conducted by Tim Van Milligan, experimental data shows that airfoiled rail buttons will have a smaller impact on the aerodynamics of the rocket than non-airfoiled ones [14]. Thus, airfoiled rail buttons are chosen based on the induced drag values of the air foiled versus regular rail buttons. The sizing of the rail buttons is constrained by the ESRA based on the guide rails used at competition, which are the size 1515 as described by subsection 9.1 of the 2017 IREC *Design, Test, & Evaluation Guide* [1]. The rail buttons chosen for the final design rocket are three delrin air foiled 1515 rail buttons from Apogee Components.

iii. RECOVERY SUBSYSTEM

1. AVIONICS OVERVIEW

The avionics serve as a controller for recovery subsystems as well as the method of data collection while in flight. The avionics are required to serve as a data acquisition system for determining and recording when apogee occurs, to initiate the separation of the rocket at apogee and again slightly below an AGL altitude of 366 m for the drogue and the main parachute respectively. They shall also include a tracking system to retrieve the rocket after it lands. It is equally important to include redundancy of the avionics to ensure parachute deployment. Included in the Avionics Selection Analysis appendix is a table documenting the numerous options available to serve these needs. The Eggtimer TRS with a backup Eggtimer Quantum is chosen as it met all the requirements while being the most economic option. It also does not require a HAM radio license and is the lightest of the options considered.

The Eggtimer TRS is made up of several components that allow the acquisition and transmission of data throughout the flight. It uses a TE/Meas-Spec MS5637 pressure sensor which is rated to approximately 70,000 ft (21,336 m) to determine altitude. It is accurate to 3 ft (0.91 m) and has a precision of 1.5 ft (0.46 m) throughout the 70,000 ft (2,1336 m) range. The data acquired from the pressure sensor is recorded as an altitude at a time interval of approximately twenty samples per second to apogee, after which it slows to two samples per second. It also uses a Maestro Wireless A2235H SiRF IV GPS module with a sample rate of one sample per second in conjunction with a Hope RF HM-TRP-915 RF module in the 909-925 Hz band to transmit altitude and GPS data to an LCD receiver. The Eggtimer TRS is rated for voltages of 3 V to 60 V for deployment, as well as a maximum current of 8 A. To ensure that there is no early or late deployment of the drogue parachute, a mathematical filter is applied to the flight data to prevent deployment due to pressure changes during Mach transition. Two batteries, one for deployment and one for the other functions such as GPS tracking, telemetry, etc. are used in the Eggtimer TRS [15]. Each of the batteries is LiPo 7.4 V 800 mAh, to allow for long waiting periods in the desert.

As the rocket is at a slight angle, it is highly unlikely that the velocity at apogee will be zero; this means it is incredibly difficult to deploy the drogue parachute at apogee. If the Eggtimer TRS [15] determines that there has not been an increase in altitude after one second, it assumes that the rocket has begun to descend. This ensures that the parachute is deployed as close to apogee as can be reliably detected. The Eggtimer Quantum [16] uses the same method for determining when the drogue parachute should be deployed. The Eggtimer Quantum serves as a backup, and is set to deploy one second after the Eggtimer TRS.

The flight computer triggers the drogue channel, which fires a charge to the igniter for two seconds. The igniter activates the black powder ejection charge which creates pressure inside the airframe. The pressure causes the shear pins to fail which allows the bottom tubing to separate from the coupler. The parachute then unravels and deploys.

When the Eggtimer TRS senses that the altitude of the rocket has dropped below 366 m AGL, it triggers the main channel which fires a charge to the igniter for two seconds. The Eggtimer Quantum serves as backup and triggers the main channel once it senses that the altitude of the rocket has dropped below 366 m. The igniter activates the black powder ejection charge which creates pressure inside the airframe. The pressure causes the shear pins to fail which allows the

nose cone to separate from the top tubing. The parachute then unravels and deploys. The deployment altitude of 366 m AGL is in compliance with subsection 3.1.1.2 of the IREC *2017 Design, Test, & Evaluation Guide* [1] which states that, "…the main deployment shall occur at an altitude no higher than 1,500 ft (457 m) AGL and reduce the vehicle's descent rate sufficiently to prevent excessive damage upon impact with ground (i.e. less than 30 ft/s [9 m/s])." Based on the parachute chosen and the deployment altitude of 366 m AGL, the rocket will be descending at a velocity of approximately 8.3 m/s.

2. PRESSURE RELIEF HOLE DESIGN

Four static pressure holes with a diameter of 0.2 in (5.1 mm) serve to equalize the pressure in the avionics bay. Multiple holes are used to prevent strong gusts of wind in any one orientation to affect the pressure sensors. As there is a fair amount of debate as to the appropriate sizing for the static pressure ports in the avionics bay, the rule of thumb is used, as recommended by Eggtimer Rocketry, the manufacturer of both flight computers. One small change is made, as Eggtimer Rocketry [15], [16] recommends three static pressure ports to eliminate the possibility of cross flow. *The Ambassador* has four ports, at equal intervals around its diameter. The sled in the avionics bay is at an angle, which serves to eliminate any cross flow. The four ports are used, as they allow access to three switches located ninety degrees from each other. This setup allows for a simpler design as no access door or other method of access is required which could have added a possible point of failure and another discontinuity along the outer surface of the airframe.

The diameter of the static pressure ports is sized to accommodate one 0.25 in (6.35 mm) diameter hole for every 100 in^3 (16.4 cm^3). Given an avionics bay with an inner diameter of 5.73 in (145 mm) and a length of 12 in (305 mm), this amounted to 0.220 in (5.58 mm) diameter holes. A 0.2 in hole was drilled due to drill bit size limitations. The Eq. (42) [17] is used to make the approximation can be found in the Vehicle Analysis appendix.

The static pressure ports [18] are over four body diameters away from the joint between the nose cone and the body tubing to allow for any pressure on the nose cone to dissipate prior to reaching the holes. This places them in the lower body tubing due to the length of the upper tubing. They are not in the direct path of any exterior features, except for the joint between the upper and lower body tubing. This eliminates the risk of turbulent flow affecting the barometric pressure sensor readings from the flight computers [17]. The static pressure ports are not in line with the flight computers [16], so the risk of currents affecting the pressure sensor is mitigated.

3. ADDITIONAL ELECTRONICS SELECTION

A Raspberry Pi and an Arduino with a separate microcontroller are created to collect information such as acceleration, orientation, and altitude. They do not count as the official altimeters. The Raspberry Pi is equipped with a BME 280 pressure sensor, and the BNO055 9-axis absolute orientation sensor. It is programmed using python. The microcontroller system is equipped with an ATmega328 microcontroller, a BMO280 pressure sensor and the BNO055 9-axis absolute orientation sensor. It is programmed using C++. Both units required wiring and programming to acquire the data from each of the sensors and store it to an SD card in a format that could be easily exported into a program such as MATLAB for analysis. All soldering was

done using lead free solder. No surface-mount soldering was required. Schematics for both units can be found in the *Engineering Drawings* Appendix.

4. PARACHUTE & DROGUE SELECTION

Parachute selection is very important for the safe recovery of the rocket. When choosing the best material to use for the parachute, it is important to consider the strength of the material, and thermal resistance. It must be able to withstand the opening shock caused by the deployment and must be able to sustain the weight of the rocket as it descends. Materials commonly used in parachutes for high powered rockets are Kevlar and Nylon. Kevlar has a decomposition temperature of 800 °F (427 °C) and a breaking strength of 435 ksi (3 GPa) [21] [20]. Nylon has a decomposition temperature of 480 °F (249 °C) and a breaking strength of 96 ksi (0.67 GPa) [20]. Nylon is a material that is more commercially available, it is also lighter in weight and cheaper.

The Design, Test, & Evaluation Guide of for the 2017 IREC states that the initial deployment event must slow down the rocket to a velocity between 75 to 150 ft/s (23 to 46 m/s) [1]. To adhere by these rules, a MATLAB code was developed to calculate the descent velocity of the rocket. To achieve a descent velocity within this range, the diameter of the required drogue is calculated. The drogue being used in The Ambassador [21] has a diameter of 48 in (121.92 cm), a coefficient of drag of 0.75, with a projected diameter of and a spill hole with a diameter of 30.57 inches (77.65 cm) and a spill hole with a diameter of 3.82 inches (9.70 cm). This slows the rocket down to about 125 ft/s (0.305 m/s).

Similarly, the formula is used to calculate the required diameter of the main parachute. The Design, Test, & Evaluation Guide of for the 2017 IREC states again that the main deployment must slow the vehicle down to less than 30 ft/s (9 m/s) [1]. The parachute that is being used is a Skyangle Cert-3 XL [22]. It has a projected diameter of 62.4 in (158.5 cm) and a coefficient of drag of 2.59. To prevent entanglement of the shroud lines, the parachute that is being used in the final rocket has only four shroud lines. From the MATLAB trajectory model, the descent velocity of the rocket is estimated to be 8.3 m/s, which follows the IREC constrains.

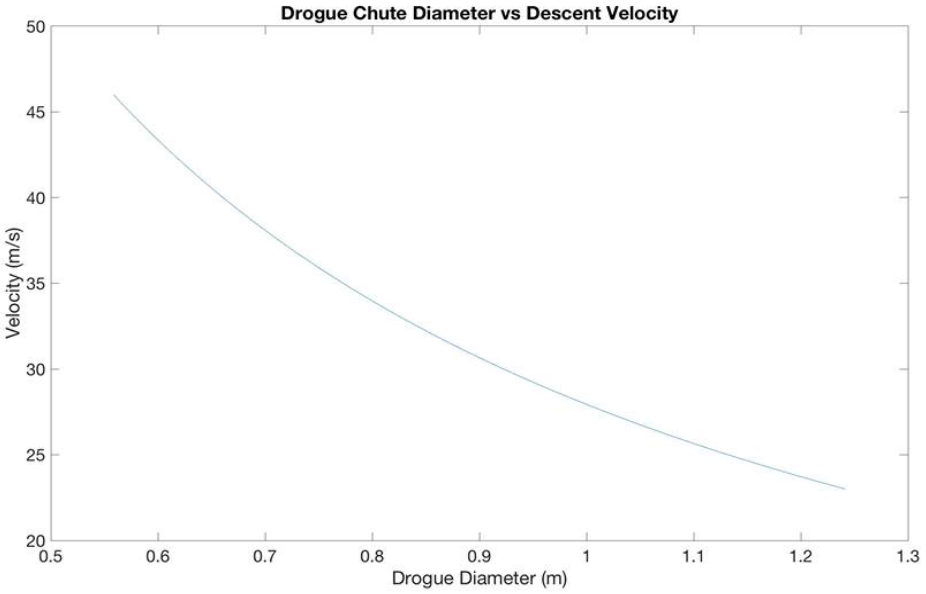

Figure 3: Descent Velocity vs Diameter of the Drogue Parachute

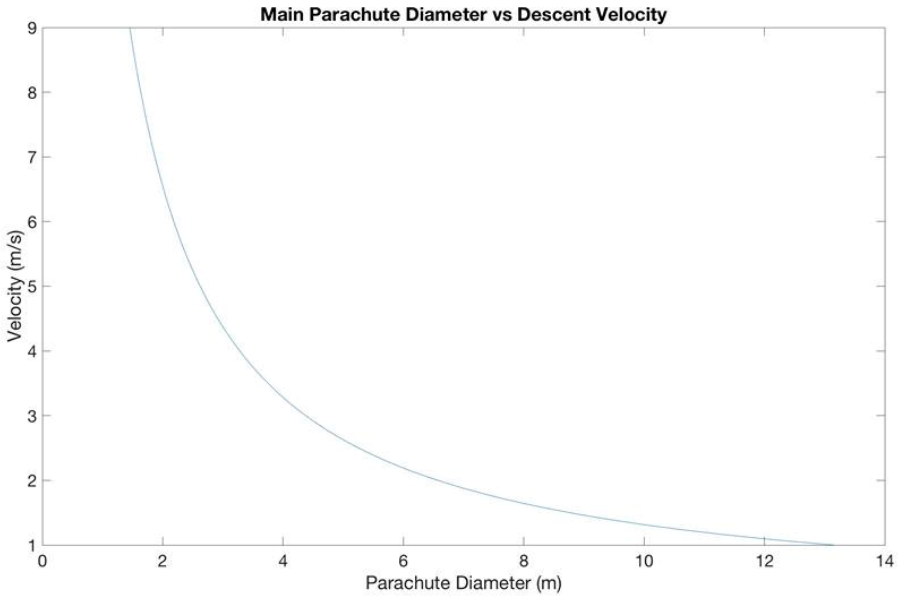

Figure 4: Descent Velocity vs Diameter of the Main Parachute

iv. PAYLOAD SUBSYSTEM

The payload bay is designed to hold at minimum 4 kg (8.8 lbs) payload using the CubeSat standard, which is one of the two required options for the design of the stowed outer mold line for IREC 2017 based on subsection 2.3.4 of the 2017 IREC Rules & Requirements Document [2]. The CubeSat standard states that the payload must be a 10 cm by 10 cm by 10 cm (3.94 in by 3.94 in by 3.94 in) cube as shown in detail in Fig. 5 as well as be able to freely slide in and out of the payload bay when not in flight. The payload must have zero degrees of freedom. The payload is

designed with the threaded holes through it so that mass can be added when needed to meet altering flight conditions.

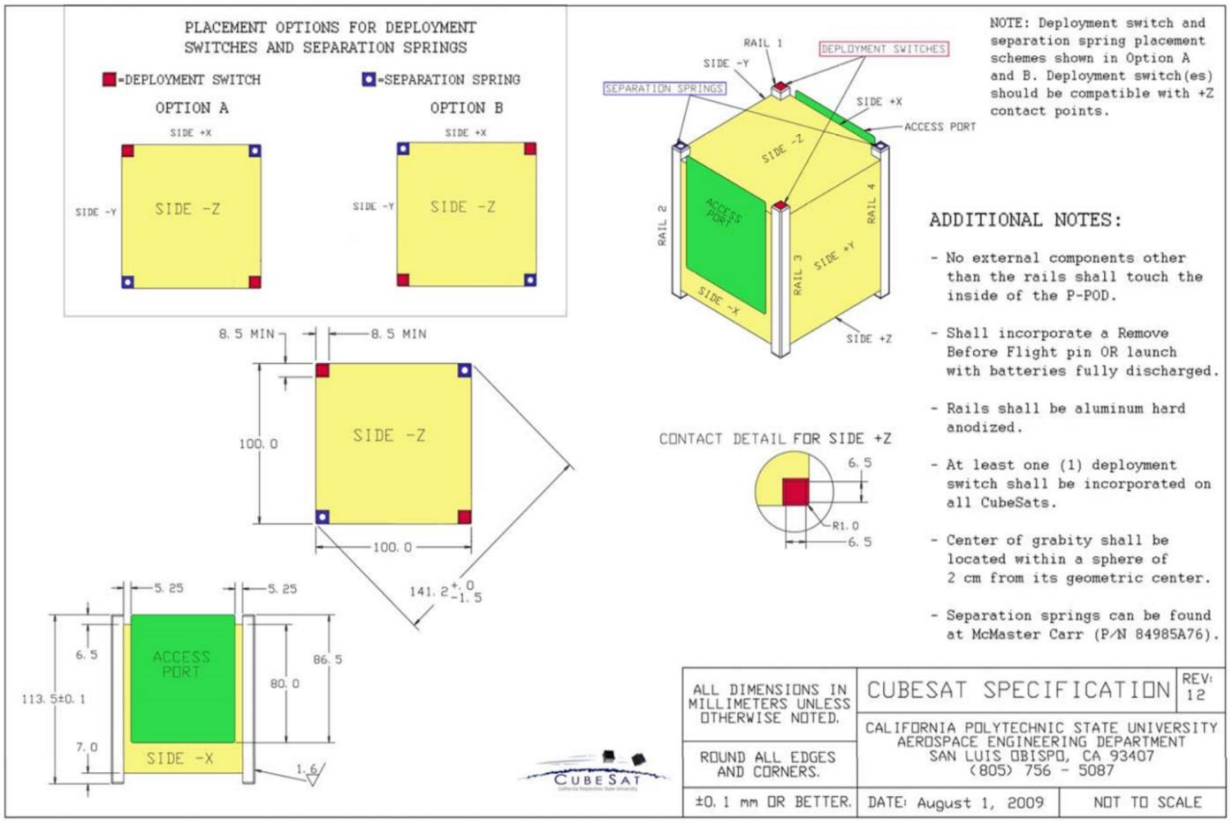

Figure 5: CubeSAT Standard [26]

VI. PHYSICAL IMPLEMENTATION

The build of The Ambassador concentrates on the construction of four major components: the airframe, the fin canister, the avionics bay, as well as the payload bay.

The upper and lower sections of the body of the rocket is cut with the use of a hydraulic band saw that ensures a straight cut that is perpendicular to the length of the tube. The cut is made at a location determined by the placement of the other internal components such as the motor, parachutes, and the additional space required for the coupler and nosecone shoulder. The coupler, nosecone shoulder, nosecone, centering rings, bulkheads, and the inner tube for the motor mount all were ordered premanufactured and cut. These pieces are acquired this way as the university has limited capabilities for fiberglass manufacturing and convenience for the centering rings and bulkheads.

The payload must be 4 kg and must follow the CubeSat standard which is a 10 cm by 10 cm by 10 cm cube with four feet on the top and bottom of approximately 7 mm cube each. The payload gets its weight from a steel block that is milled down to a few hundred grams above 4 kg. Plywood is then cut to fit over the steel block to fulfill the dimension requirement. Once the dimension requirement is fulfilled holes are drilled into the block to reduce the weight to the approximate

amount. The holes are then tapped so that additional weight can be inserted as the drilling and tapping process can make it difficult to reach exactly 4 kg exactly. The insertion for additional weight also makes for the opportunity to increase the weight based on flight conditions.

The design of the payload bay consists of a bulkhead made from half-inch plywood that is epoxied into the nose cone. Rails are made from a one-inch diameter maple wood dowel with a slot cut out with a cross section of a 5 mm square. The rails are then attached to the disk and epoxied onto the inner surface of the nosecone. These rails prevent the payload movement and eliminate all degrees of freedom. This allows for the payload to be inserted into the nosecone and removed when the rocket is not in use. The bottom bulkhead of the payload bay is secured into the shoulder of the nosecone. The shoulder is then attached to the nosecone with four well-nuts. Well-nuts are a rubber tube with a nut fixed in it so that when a bolt in inserted and tightened the rubber is compressed to firmly secure the bolt in place. This type of bolt is used as it does not add any sharp edges to the inside of the rocket for the recovery system to potentially tear on. The lower part of the nosecone shoulder has six holes drilled and tapped through and are aligned with the top body that hold the large shear pins.

Finite Element Analysis (FEA) shows that the weakest location of the payload bay is at the point of contact between the payload and the bottom bulkhead. Due to the geometry of the nosecone, the top bulkhead does not move further into the nosecone. The bottom bulkhead is the only part that is susceptible to motion during the powered portion of flight. The bulkhead is made of half inch plywood with a fiberglass bulkhead epoxied to the bottom. This combination provides a solid mounting surface for the U-bolt used in the recovery system but also provides sufficient contact surface area to the nosecone shoulder to prevent shear. Calculations have been conducted to show that the epoxy will not shear at this location. The force calculations are done using the maximum G force to which the rocket is subject to withstand during maximum acceleration. Both the top and bottom bulkheads have a cross added to them to increase the rigidity of the bulkheads.

Due to the choice in flight computers, it is required to solder the provided components together for the Eggtimer TRS, Eggtimer Quantum and Eggtimer LCD. This is done with through-hole and surface-mount soldering by hand. This soldering is completed using 0.020 in (0.050 cm) no-clean low-temperature solder to ensure no damage to the parts. All of the components were provided by the manufacturer as well as clear assembly instructions. Care is taken to ensure that the GPS module and other critical components are not to experience too much heat. No plug-in components or friction fit components are used in the construction of the flight computers. The soldered components are then fixed with small bolts and zip ties to what is known as the sled. The sled is a piece of pressboard wood and is attached to two threaded rods with steel clamps that have rubber dampeners on them to help reduce any vibration to the electrical components. Hex nuts are used to keep the sled in its proper position on the threaded rods. There is a fiberglass bulkhead at each end of the electronics bay where the threaded rods are attached with wing nuts with plumbers' putty sandwiched between the bulkhead and the bottom of the nut. Each fiberglass bulkhead has a U-bolt bolted through and epoxied into place for the recovery system to be attached. There are also two PVC pipe caps epoxied to each bulkhead to hold the main and back up black powder charges for the drogue and main parachutes. The sled is placed inside of the coupler for the top and lower body of the rocket where the bulkheads rest on the top edge of the coupler. The electronics coupler is attached to the upper body with four well nuts and is attached to the lower body with six 2-56 shear pins.

One of the main challenges with the construction process is ensuring the accuracy of the marking and drilling of the vent and bolt holes for the rail buttons, shear pins and well-nuts. This is a challenge as the bolt holes cannot line up with the vent holes and the holes. The placement of all the holes is marked on a piece of paper with the degrees marked in a circle to ensure there is no interference of the airflow. Using the location of the rail button as a reference point since they line up on the top and lower bodies, the holes were marked on the middle body and then drilled. The coupler and nosecone shoulder are then placed in their appropriate and the correct depth of half the coupler and nosecone shoulder. The holes are drilled one at a time again through the second component placing the correct fastener into the hole after it is drilled to ensure the component does not spin in the upper body while the holes are being drilled. This process is repeated for the lower body and the nosecone, the coupler and the nosecone shoulder are left connected to the upper body so the holes across the rocket will line up with minimal error. The only holes that are tapped are the holes for the shear pins.

The motor mount is in the base of the rocket and is made up of three fiberglass centering rings and a fiberglass bulkhead at the top. The top bulkhead has a through U-bolt epoxied to it to attach the shock cord and parachutes. The centering rings are evenly spaced out and are epoxied to the body tube. The centering rings are also epoxied to an inner tube that will hold the motor casing. There are three threaded rods that go through the centering rings and the top bulkhead with hex nuts securing the rod to each component. The threaded rods also secure the thrust plate to the lip of the bottom body, the thrust plate also is epoxied into place. The thrust plate then has the inside component piece of the retaining ring bolted to it. The remaining half of the retaining ring is tightly twisted into place once the motor casing with the motor and nozzle attached is placed into the rocket.

Three slits are cut into the bottom of the bottom body 120 degrees apart for the fins. The slit is also placed in the middle centering ring. The fins are CNC cut to the appropriate shape out of flat fiberglass plates. The fins are cut so that they sit on the top and bottom centering rings and flush against the inner tube. A fillet is cut on the leading edge of each fin with hand held power tools as the CNC machine is unable to make this cut. The fins are epoxied to each point of contact to secure them initially. Once the fins are firmly attached a one-inch fillet of epoxy is added to each side of the fins to firmly attach them to the body.

When the rocket body and couplers are complete the main parachute and drogue parachute are inserted. These parachutes are purchased from a supplier prefabricated. The main parachute is tied to the centre of the shock cord. The loose ends are tied to the U-bolts located in the nosecone shoulder and the top of the coupler that holds the electronics bay. The drogue parachute is tied to the shock cord in the centre as well. Its loose ends are then tied to the U-bolts located at the top of the motor mount and at the bottom of the coupler of the electronics bay.

VII. EXPERIMENTAL RESULTS

i. AIRFRAME BODY TUBING TEST PROCEDURES AND RESULTS

Material testing is conducted on phenolic tubing, quantum tubing and fiberglass wrapped phenolic tubing. Material testing for the listed body airframe materials is necessary as material properties are not available for these materials. Four-inch diameter tubes were donated by Public

Missiles Ltd for testing of these materials. It is assumed in the results that the curved nature of the specimens caused a loss in strength. Results from these tests in the tables featured in this appendix.

The ASTM standard D638-14 Standard Test Method for Tensile Properties of Plastics was used to conduct the tensile tests. This method was selected due to its applicability to thermosets, phenolic molded resin, laminated materials, and resin-matrix composites of thicknesses between 1.0 mm and 14 mm [23]. Specimens are cut from the provided tubing specimens using a bandsaw and rotary tool. These samples were tested using a MTS Criterion Series universal testing machine with tensile clamp extensions.

The ASTM standard D2344/D2344M-16 Standard Test Method for Short-Beam Strength of Polymer Matrix Composite Materials and Their Laminates was used to conduct the bending tests. It was selected due to its applicability to curved specimens less than 6 mm thick. As this standard took curvature into consideration and two thirds of the tubing materials are composites, this method was used for testing [24]. Samples are cute to a fixed length of 4 cm using a bandsaw and rotary tool. These samples were tested using a MTS Criterion Series universal testing machine with a three-point bend testing extension.

The results for both testing procedures are presented in the following tables:

Table 2. Result Summary of Three-Point Bend Testing

Material	Tests	Maximum Load (N)	Average Maximum Load (MPa)	Maximum Strength (MPa)	Average Strength (MPa)	Standard Deviation	Coefficient of Variation
Phenolic	0->5	92.0231	83.9878	3.1486	2.8737	0.2592	0.0902
Quantum	6->11	116.2472	108.7789	3.9774	3.7219	0.2163	0.0581
Fibre-glassed Phenolic	12->17	126.6049	104.0385	4.3318	3.5597	0.4730	0.1329

Table 3. Result Summary of Tensile Testing

Material	Tests	Maximum Load (N)	Maximum Tensile Strength (MPa)	Average Tensile Strength (MPa)	Standard Deviation	Coefficient of Variation
Phenolic	1->5	300.8221	31.3356	28.1558	2.7013	0.0959

Material	Tests	Maximum Load (N)	Maximum Tensile Strength (MPa)	Average Tensile Strength (MPa)	Standard Deviation	Coefficient of Variation
Quantum	6->10	466.0280	43.1507	39.4766	3.2687	0.0828
Fibre-glassed Phenolic	11->15	800.82863	66.7357	57.9284	5.6619	0.0977

ii. RECOVERY SYSTEM TESTING

Three flight computers are used for data acquisition and parachute deployment. The avionics system used for parachute deployment consists of a flight computer called the Eggtimer TRS paired with the Eggtimer Quantum. These two flight computers also record altitude and velocity with respect to time, as well as initial altitude above sea level, initial temperature, as well as time and altitude at both parachute deployments. The third flight computer is an Arduino based microcontroller with several chips used to record altitude, time, and orientation throughout the flight.

As the flight computers are almost entirely hand soldered, it is important that testing occur throughout the process to ensure that if something did not go as planned, that there would be sufficient time to correct it. In testing, members stood outside with a partially built Eggtimer TRS to test the GPS and RF transmitter to verify functionality. This is done primarily to ensure that there are no problems with the assembly, prior to soldering the microcontroller over several surface-mount soldered resistors. After the Eggtimer TRS, Eggtimer Quantum and Eggtimer LCD are built, the charges are tested using Christmas tree lights as resistors, as recommended by Eggtimer. This ensured the electronics are functional before the rocket is built.

The deployment system is verified based on the methods suggested by Eggtimer, the manufacturer of the flight computer used. This is done through ground tests conducted after the rocket is built. Careful consideration to safety precautions during testing is necessary due to the usage of black powder. Nitrile gloves, safety masks and safety glasses are used, and a fire extinguisher is accessible and present when handling black powder.

In flight, the avionics will sense that the rocket has reached apogee and will send an electronic charge to an igniter which will be in contact with a set amount of black powder. One second later, the redundant system will set off another electric charge to an igniter which will be in contact with this same canister of black powder.

To reproduce this in a test environment, the rocket is set up as if it were to be flown, except for the motor which does not need to be included for the test. The rocket is then placed on a fixture which ensures that it will not move. The main flight computer and radio frequency receiver is turned on and paired. At a safe distance from the rocket, a radio frequency receiver is used to ignite the black powder charge through a built-in test function. This is repeated for both the drogue and

main parachutes using the main flight computer. This test ensures that there is enough black powder to cause a successful parachute deployment and that the flight computer, shear pins, canisters, and igniters are working correctly.

An equivalent mass is used to simulate the volume and weight of the parachute and shock cord to protect them from the black powder, as there is a possibility that the amount of black powder determined through rule of thumb and calculations would be much too high. Primary testing was conducted after a long night of rain, and thus was conducted on moist ground, reducing the risk of fire. This primary test resulted in 3.2 grams of black powder used for the deployment of the main parachute and 2 grams of black powder used for the deployment of the drogue parachute. One gram of black powder is added to both the main and drogue backup charges, which results in 4.2 grams and 3 grams of black powder respectively.

The main parachute deployed prematurely in the first launch of The Ambassador, which caused the rocket to land on top of a tree approximately six and a half kilometers away. The reason that the screws sheared prematurely was that the force caused by the falling nosecone was greater than the force required for shearing. Prior to the second launch of The Ambassador, the shear pins for the main parachute deployment were replaced with much larger shear pins, requiring additional black powder testing. This second round of testing showed that 8 grams of black powder was too high and caused failure in other parts of the rocket. The black powder used for the drogue parachute remained unchanged, with 2 grams of black powder used for the deployment and 3 grams of black powder used for the backup charge. For the second launch of *The Ambassador*, 7 grams of black powder was used for the deployment of the main parachute and 7.5 grams of black powder was used as a backup charge.

iii. IREC 2017 COMPETITION RESULTS

The following table summarises the performance results of the University of Windsor Rocketry Team at the 2017 IREC. Out of 45 participating teams in the *10k – COTS – All Propulsion Types* category, the team placed 3rd in the category while placing 3rd overall in the whole competition among 82 teams. *The Ambassador* successfully launched at competition and was safely recovered, with a recorded peak AGL altitude of 3210.5 m. In the following section, *Design Specifications and Performance Metrics,* the performance score breakdown is further described.

Score Category	Admin Subtotal (max. 100)	Project Technical Report (max. 200)	Design Implementation (max. 200)	Flight Performance (max. 500)	Penalties	Total Score (out of 1000)
Score	100	185	122.5	406.725	0	814.225

Table 3: IREC 2017 10k – COTS – All Propulsion Types Category Results

VIII. DESIGN SPECIFICATIONS AND PERFORMANCE METRICS

The following table shows the key design specifications used to evaluate the launch of *The Ambassador*.

Table 4: The Ambassador Report Flysheet Summary

***The Ambassador* Report Flysheet Summary**	
Vehicle Properties	
Total Length (in/m)	95.9/2.45
Diameter (in/m)	6/0.152
Gross Lift Off Weight (lb/kg)	54.3/24.6
Airframe Material	G-10 Fiberglass
Fin Material	G-12 Fiberglass
Coupler Length (in/m)	12/0.305
Selected Nose Cone	6 in (15.24 cm), 5.7-1 Von Kármán
Motor Properties	
Motor Designation	M1845NT
Max/Average Thrust (lb/N)	693/421 3081/1875
Total Impulse (N-s/lb-s)	8307/1867.5
Mass Before/After Burn (lb/kg)	54.23/45.85 24.5/20.83
Liftoff Thrust (lb/N)	505.8/2250
Motor Retention	Aerotech 98 mm Retainer
Burn Time (s)	4.4
Stability Analysis	
Centre of Pressure (in/m)	71.3/1.81
Centre of Gravity (in/m)	59.06 /1.50
Static Stability Margin	1.99
Static Stability Margin (off launch rail)	1.99
Thrust-to-Weight Ratio	9.2
Rail Length (ft/m)	18/5.49
Rail Exit Velocity ([ft/s]/[m/s])	96/29.6
Ascent Analysis	
Maximum Velocity ([ft/s]/[m/s])	966/294
Maximum Mach Number	0.86
Maximum Acceleration (ft/s^2) (m/s^2)	305/93
Target Apogee (ft/m)	10000/3048
Predicted Apogee (ft/m)	10137/3089
Stable Velocity ([ft/s]/[m/s])	-
Time to Apogee (s)	26

Recovery System Properties	
Drogue Parachute	
Manufacturer/Model	Spherachutes
Size (in/m)	48/1.22
Altitude at Deployment (ft/m)	10137/3089
Velocity at Deployment ([ft/s]/[m/s])	0/0
Terminal Velocity ([ft/s]/[m/s])	121/37
Recovery Harness Material	Tubular Nylon
Harness Size/Thickness (in/cm)	0.5/54
Recovery Harness Length (ft/m)	28.133/8.575
Harness/Airframe Interfaces	1/2" U-bolt attached to after payload bulkhead

Recovery System Properties	
Main Parachute	
Manufacturer/Model	SkyAngle
Size (in/m)	109/2.76
Altitude at Deployment (ft/m)	1000/304
Velocity at Deployment ([ft/s]/[m/s])	121/37
Terminal Velocity ([ft/s]/[m/s])	27.3/8.3
Recovery Harness Material	Tubular Nylon
Harness Size/Thickness (in/m)	0.5/54
Recovery Harness Length (ft/)	28.133/8.575
Harness/Airframe Interfaces	1/2" U-bolt attached to after payload bulkhead

Recovery Electronics	
Altimeters(s)/Timer(s) (Make/Model)	Eggtimer TRS
Redundancy Plan	Eggtimer Quantum
Pad Stay Time (Launch Configuration)	-

Recovery Electronics	
Altimeters(s)/Timer(s) (Make/Model)	-
Redundancy Plan	-
Pad Stay Time (Launch Configuration)	-

Payload	
Payload Type	Steel
Weight (lb/kg)	8.81/4
Type	CubeSat Standard Payload

The scoring of the 2017 IREC is based on a 1000-point performance system in which half of the points are allocated towards the performance of the launch. Table 5 goes over the breakdown of the point scoring system used in competition.

Table 5: 2017 IREC Performance Scoring System

Score Category	Maximum Allocated Score	Description
Admin Subtotal	100	- Correct, complete, and timely delivery of the team's entry form and all progress updates, where each entry is valued at 25 points.
Project Technical Report	200	- 40 points are allocated for the completeness of the report - 120 points for the analysis - 40 points for the correctness of the presented report information.
Design Implementation	200	- 100 points are allocated towards the competency and design implementation - 100 points are for the degree of student research and development (SRAD), specifically with the fins, airframe, parachutes, and other components.
Flight Performance	500	- 350 points related to the flight performance are based on how close the rocket was to reaching the target apogee, calculated in the following equation: $Points = 350 - \left[\frac{350}{2{,}000}\right] \times \left\lvert Apogee_{Target} - Apogee_{Actual} \right\rvert$ - Successful recovery is worth 150 points with no excessive damage
Penalties	-	- teams may be penalized 20 points off their total score for every unsafe or unsportsmanlike conduct recorded by IREC officials
Total Score	1000	-

IX. PROOF-OF-DESIGN-CONCEPT DEMONSTRATION

i. COMPUTATIONAL FLUID DYNAMICS ANALYSIS

Computational fluid dynamics (CFD) software, ANSYS Fluent 17.0 [25], is used to simulate the fluid flow around three-dimensional bodies such as a rocket, and can easily solve complex models such as transonic compressible flows. Such a simulation is essential to visualize the flow at the following critical points along the rocket: the nose cone tip, around the fins and along the body of the rocket. A three-dimensional up-to-scale CATIA model of *The Ambassador* is imported into the ANSYS Fluent Workbench that excludes the rail buttons, vent holes, shear pins and screws. At an estimated maximum Mach number of 0.81 and a maximum angle of attack of 5 degrees from the y-axis along the xz-plane of the figures below, a steady CFD simulation is created. This flight condition is estimated to be encountered at the end of the burn phase, representing its "worst case" scenario where peak Mach numbers are achieved. The corresponding atmospheric properties at this point in flight are assumed and simulated.

A 20 m radius hemispheric fluid body and a 40 m extrusion symmetrically surround the rocket to ensure accurate boundary layer and flow modelling. Each face of the rocket is modelled as a no-

slip wall with a surface roughness height of 20 μm. The outer surfaces of the fluid body are modelled as pressure far-field. A body of influence of 0.75 m radius symmetrically surrounding the rocket is created to facilitate inflation and ANSYS's overall meshing capabilities. A fine mesh at the surface is created to increase the accuracy of the results on the faces of the rocket. Inflation is added to the mesh to gradually increase the element size from a fine mesh at the wall to a course mesh at the outer edges of the large fluid body.

The actual model setup involves using the energy equations and the Spalart-Allmaras viscous model [26]. Table 6 to 8 summarize the main details of the Design Modeler, the meshing window, the Fluent setup, and the important results. Subsequently, contours for the coefficient of pressure and the isentropic Mach number at the nose tip and fins are shown in Figures 7 to 12. Figure 7 highlights a relatively high pressure distribution at the nose tip and confirms the selection of a metallic nose tip for the final design. On the other hand, Figure 8 shows a rapid decrease in coefficient of pressure at the trailing edges of the fins on the high-pressure side. This indicates the presence of shocks at these locations which contributes to wave drag [7]. These could have been avoided by decreasing the chamfer angle of the trailing edges of the fins. Unfortunately, due to the time constraint before the competition, these intended changes were not made.

Table 6: CFD Mesh Specifications

Mesh	
Element Type	Triangle
Number of Elements	4326043
Number of Nodes	800340
Element Size at Wall	0.003 m
Element Size at Body of Influence Boundary	0.1 m
Inflation	Smooth Transition
Maximum Layers	5
Growth Rate	1.2

Table 7: CFD Fluent Setup

Fluent Setup	
Solver	• Pressure-Based Steady • Absolute Velocity
Model	• Energy Equation • Spalart-Allmaras Viscous Model
Materials	• Fluid: Air • Density (kg/m^3): Ideal gas • Specific Heat (j/kg-K): 1006 • Viscosity (kg/m-s): 1.60e-05

Fluent Setup	
Boundary Conditions	*Wall:* • No slip • Stationary wall • Roughness height (μm) = 20 *Pressure Input & Output:* • Gauge Pressure (Pa) = 94473 • Mach Number = 0.808 • X-Component = -0.0872 • Y-Component = 0 • Z- Component = -0.996 • Temperature (K) = 302
Reference Values	• Area (m^2): 0.0191 • Density (kg/m^3): 1.09 • Length (m): 0.156 • Pressure (Pa): 94473 • Temperature (K): 302 • Velocity (m/s): 281 • Viscosity (kg/m-s): 1.60e-05 • Ratio of specific heats: 1.4
Solution Methods	• Pressure-Velocity Coupling Scheme: Coupled • Pseudo Transient • High Order Term Relaxation
Monitors	• Coefficient of drag • Coefficient of lift
Calculation	• 155 iterations until converged solution • Approx. 5 hours

Table 8: CFD Results

Results	
Pressure Drag Coefficient	0.297
Viscous Drag Coefficient	0.185
Total Drag Coefficient	0.482

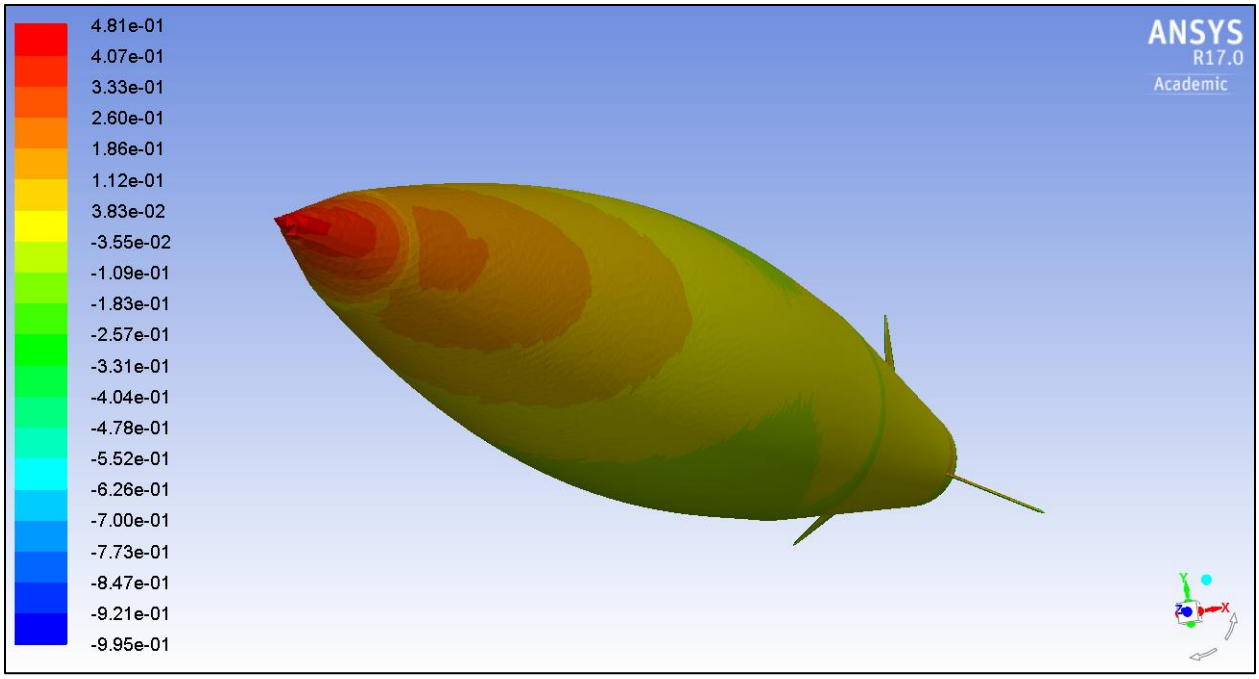

Figure 6: Coefficient of Pressure: Nose Tip

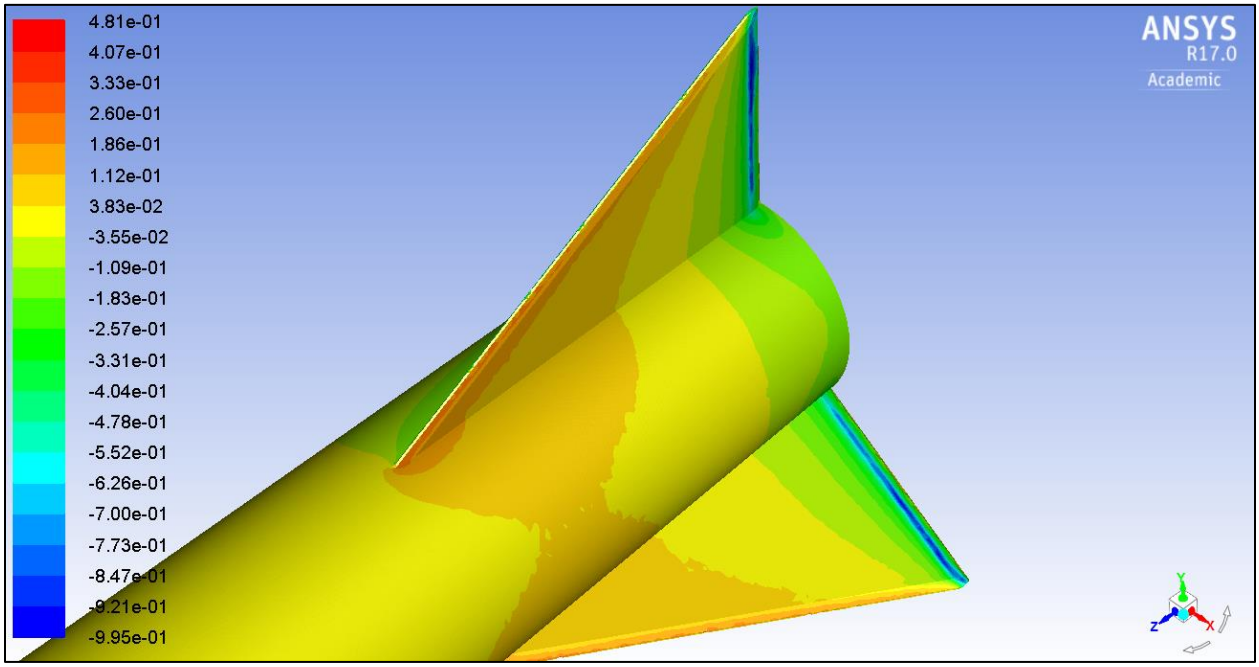

Figure 7: Coefficient of Pressure: High Pressure Side

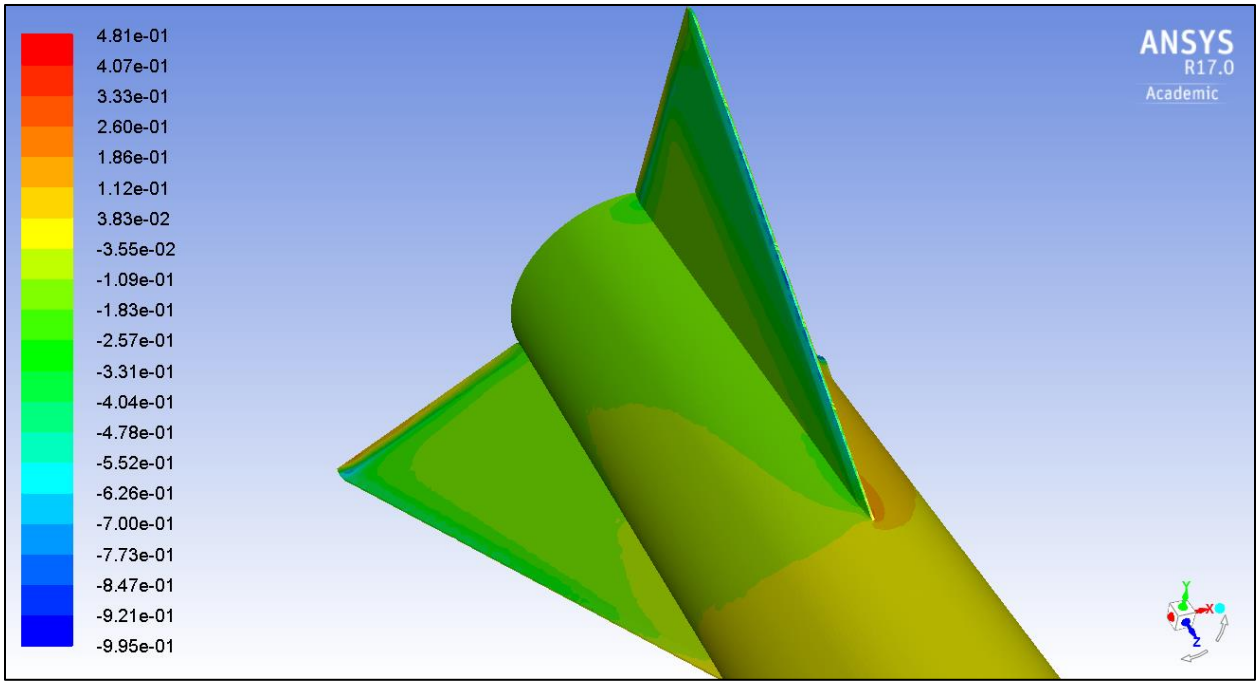

Figure 8: Coefficient of Pressure: Low Pressure Side

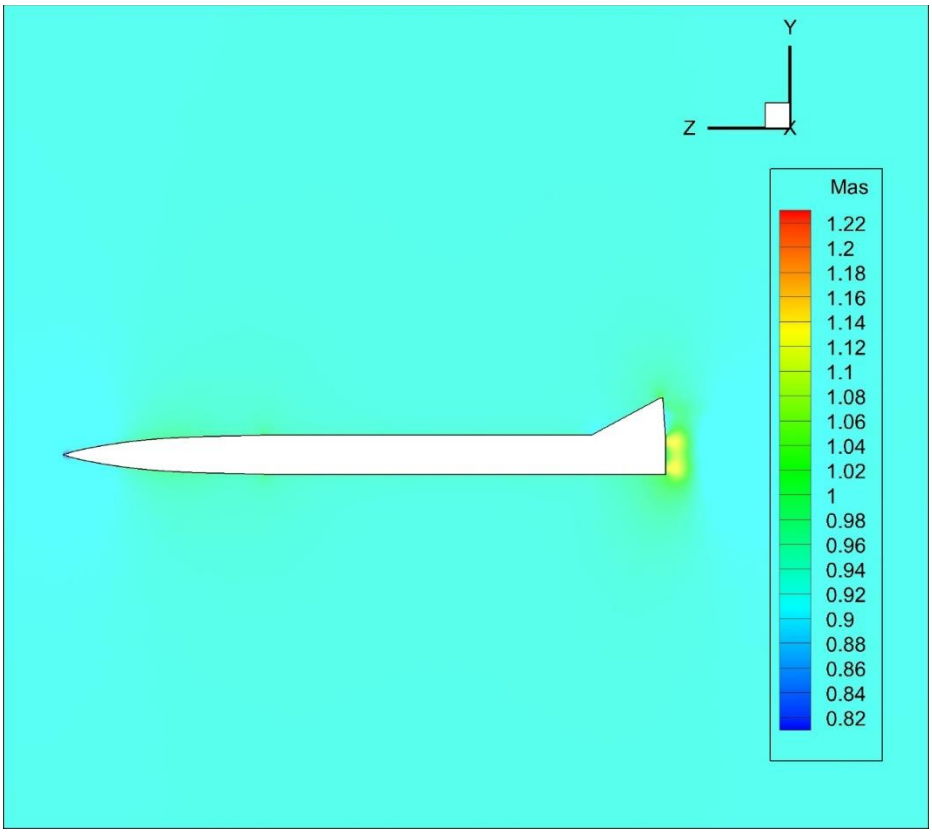

Figure 9: Isentropic Mach Number: Side View (High Pressure Side)

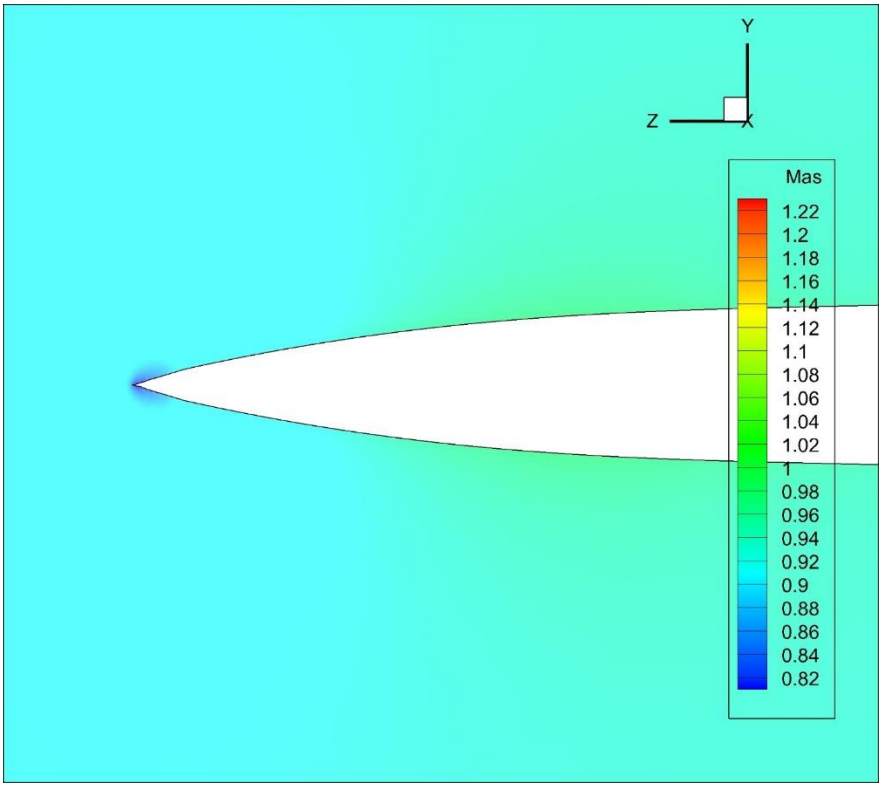

Figure 10: Isentropic Mach Number: Nose Tip

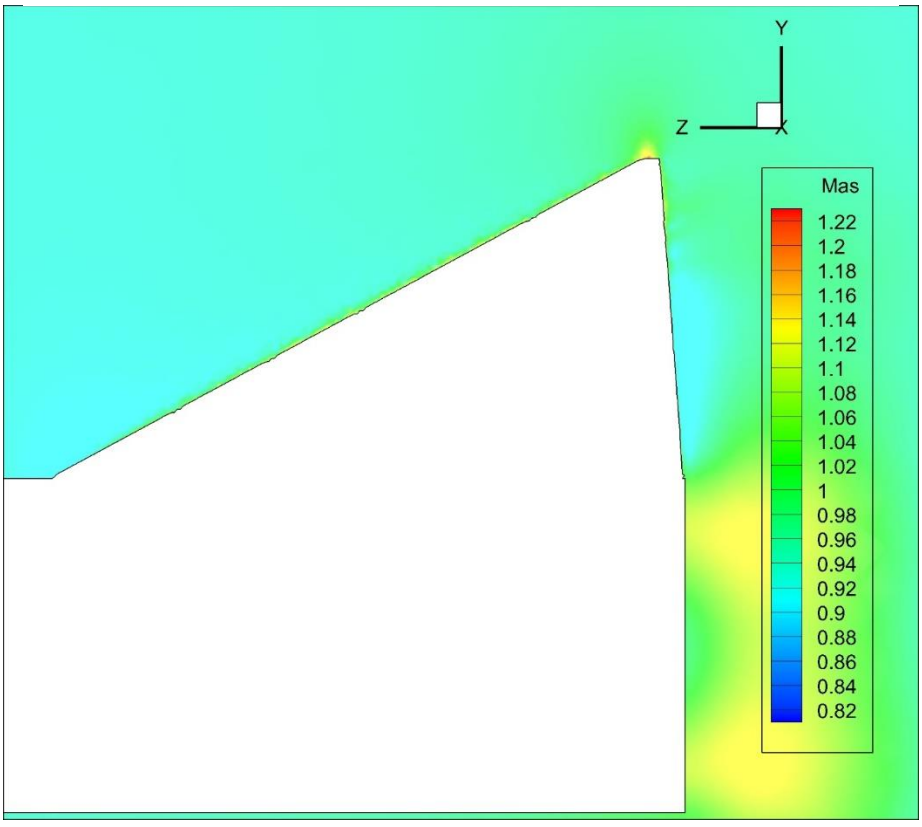

Figure 11: Isentropic Mach Number: Top Fin Side View (High Pressure Side)

ii. RESULT OVERVIEW

It is very important to validate the dynamic prediction model. To do this, two graphs are developed to compare the data from the main flight computer, the Eggtimer TRS, and the dynamic prediction model. Figure 13 shows the altitude with respect to time. The black line represents the dynamic prediction model with a 10 µm surface roughness. The grey shaded area represents the range of values given by the dynamic prediction model over a range of surface roughness from 5µm to 15µm. This is done as the surface roughness of the rocket has not been measured for the rocket after painting and the application of vinyl decals.

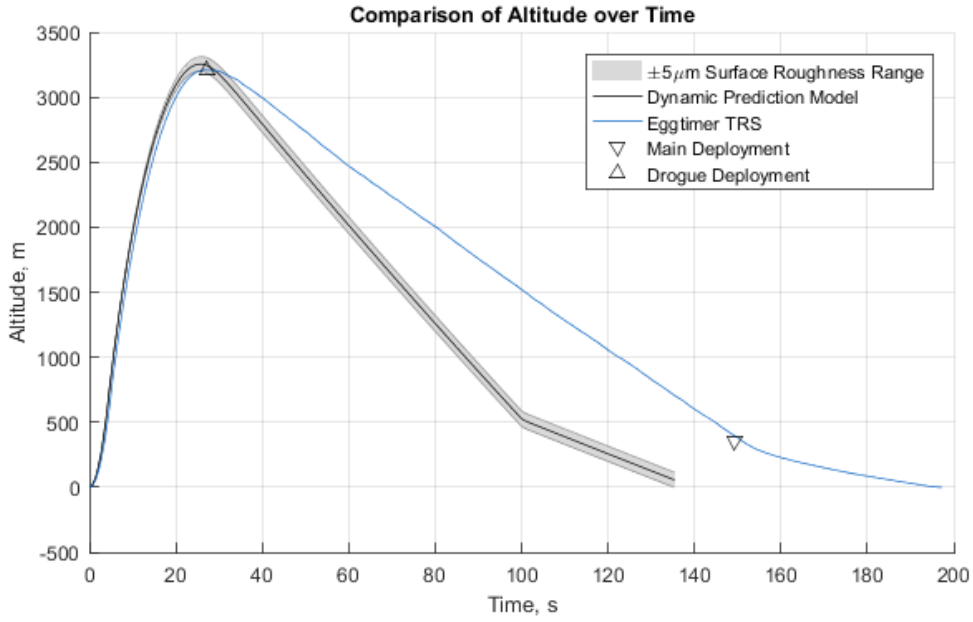

Figure 12: Comparison of Altitude over Time between Dynamic Prediction Model and Eggtimer TRS

Figure 14 shows velocity with respect to time, and is similar to Figure 13 as it closely matches the data acquired by the dynamic prediction model and the Eggtimer TRS. Figure 14 shows velocity with respect to time. The grey shaded area represents the range of values given by the dynamic prediction model over a range of surface roughness from 5 µm to 15 µm. In this figure, the variation due to surface roughness height is smaller than with the previous figure.

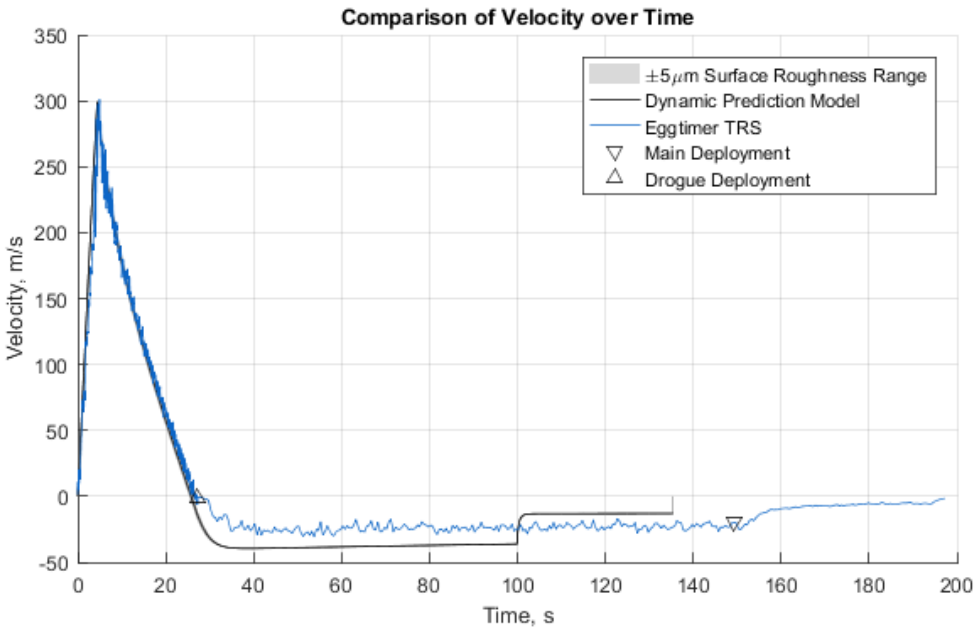

Figure 13: Comparison of Velocity over Time between Dynamic Prediction Model and Eggtimer TRS

Figure 15 shows a comparison of the three flight computers present on board *The Ambassador*. This figure shows the lack of discrepancy between three different barometric pressure sensors. This is meant to show the validity of the data obtained from each flight.

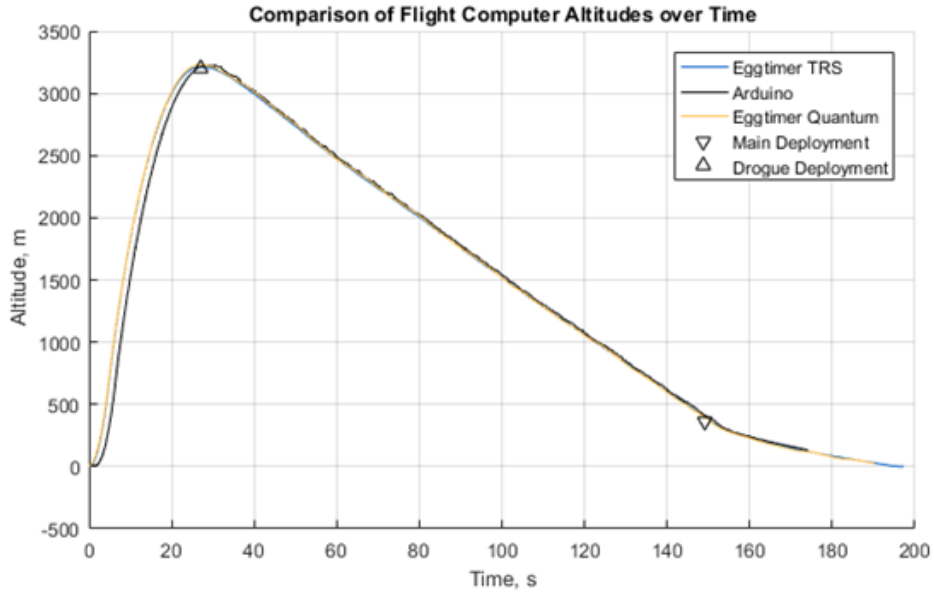

Figure 14: Comparison of Flight Computer Altitudes over Time

Table 9 shows the data from the dynamic prediction model, labeled prediction, as well as data from the on-board flight computers and data from two commercially available programs. The table also shows the error between the Eggtimer TRS and the dynamic prediction model. The Eggtimers use mathematical nose filters which smooth the noise from pressure readings, which allow for a more accurate velocity profile. This is shown in the "filtered" rows below, and explains why the unfiltered velocity has such a high error.

Table 9: Result Summary Comparison

	MATLAB	**TRS**	**Percent Error**	**Quantum**	**Arduino**	**RockSIM Prediction**	**OpenRocket Prediction**
Altitude [m]	3212.94	3210.46	0.08	3229.66	3229.00	3733.61	3431.13
Filtered Altitude [m]	3212.94	3208.51	0.14	3229.31	0.00	3733.61	3431.13
Velocity [m/s]	295.49	463.30	56.79	463.30	0.00	292.40	287.54
Filtered Velocity [m/s]	295.49	300.65	1.75	298.30	0.00	292.40	287.54

Table 10: Result Summary Software Comparison

Rocket	**Actual Apogee (TRS data) [m]**	**RockSIM Prediction Apogee [m]**	**% Error**	**OpenRocket Prediction Apogee [m]**	**% Error**	**MATLAB Prediction Apogee [m]**	**% Error**
***Icarus* I350**	867.00	968.00	11.65	880.00	1.50	879.00	1.38
***Icarus* J285**	1018.00	1067.00	4.81	1030.00	1.18	1089.00	6.97
Ambassador M2100	2903.56	3145.27	8.32	2978.24	2.57	2792.92	3.81
Ambassador M1845	3210.46	3733.54	16.29	3431.18	6.87	3212.94	0.08

iii. FOURIER NUMBER ANALYSIS

One of the measurements that could not be recorded by the on-flight computers is the change in the temperature profile. The reason for this is that the rocket only took around 25 seconds to reach apogee. This time was insufficient and did not allow for heat transfer to occur. To confirm that this is indeed the problem, a heat transfer analysis must be conducted. To do this, the Fourier number is found. The Fourier number is a dimensionless parameter used to quantify the rate of heat transfer through a medium. It is defined as the ratio between the rate of heat transfer and the rate of heat storage. Since the rocket's velocity and altitude change over time, the approach to finding the Fourier number is simplified, and average values are used. The calculations for the Fourier number were conducted at a temperature of 32 degrees C and a velocity of 121 m/s. Properties such as the kinematic and dynamic viscosity, density, specific heat, Prandtl's number and thermal conductivity coefficient are found for air at 32 degrees C.

According to Eq. (48), the only variable that isn't available is the heat transfer coefficient "h". This is a value that is essential to finding the Fourier number. The process for finding this value included calculating the Reynolds number using Eq. (8) which falls within the range of transitional flow. Once this is done, the Nusselt number is calculated using Eq. (46). Since there is a direct relationship between the Nusselt number and the heat transfer coefficient from Eq. (47), it is easy to calculate the value for "h". This value for "h" is then used to calculate the Fourier number using Eq. (48). The calculated value for the Fourier number is $9.2x10^{-2}$. As defined, the Fourier number is a ratio measuring the rate of heat transfer to the rate of heat storage. A smaller Fourier number indicates a longer time for the occurrence of heat transfer. This result proves why the flight computers did not capture a temperature change as the rocket ascended to apogee too rapidly [27].

X. CONCLUSIONS & RECOMMENDATIONS

The primary conclusion to be made is the placement of *The Ambassador* in the IREC SAC. *The Ambassador*, and in turn, the University of Windsor Rocketry Team, placed third in both the 10K COTS category and overall in the competition out of 82 teams. An overall score of 814 out of a possible 1000 points was obtained. These are the final results to the initial objectives set out, and are especially impressive for a team from the University of Windsor that has never before participated in this competition.

In terms of the dynamic prediction model, the data acquired from the Eggtimer TRS, as well as the other two flight computers, prior to apogee show high agreement with the dynamic prediction model. This is further proof of the measured performance comparing well to the desired prototype performance specifications.

In terms of innovative contributions, the dynamic prediction model aimed to go above and beyond the current commercially available software. It has accomplished this by using a coefficient of drag that is calculated, as opposed to an iterative approach which uses data from launches, it also considers contributions to drag such as parasitic drag which is not considered in the commercially available software. The dynamic prediction software is also highly customizable, and allows the user to enter boundary conditions, temperature profile, input conditions, and change variables such as a measured surface roughness height. This is further validated by the agreement between the flight data and the dynamic prediction model which has not been shown in commercially available software.

The model was chosen for presentation as a podium session as part of IREC SAC. This is an honour and a testament to the novelty of the dynamic prediction model. The University of Windsor was one of 24 teams chosen to present out of a total of 115 teams.

i. RECOMMENDATIONS

This project is important to engineering education as it encourages students to become involved in the physics, mathematics, and engineering behind the design of a high-power rocket. This capstone project promotes the relatively new aerospace option featured in the list of undergraduate mechanical engineering programs offered at the University of Windsor, and will motivate new students to pick this option for their degree.

For future capstone teams, many recommendations can be made for project improvement and for future works. One task would be to further develop the dynamic prediction model to increase its accuracy. The importance of all the added complexities is to make the model more modular, more configurable and easier to modify than competing commercially available prediction models. Depending on the application of the code, flight complexity and accuracy required, various parameters can be modified to suit the individual's needs. Additional work would include further modifying and refining the prediction model using supplementary research and comparisons to experimental flight data that will be gathered from future launches. Before launches, air properties and other flight conditions will be detailed extensively to see how varying parameters affect flight. An uncertainty analysis on various parameters such as thrust, atmospheric lapse rate, among many others, would be beneficial for more realistic trajectory modelling.

A major recommendation for future capstone teams would be to participate in the payload challenge in upcoming years. As the University of Windsor did not attend IREC prior to this year, it was a priority to build a rocket and launch. In future years, the objectives should include the additional challenge, as it is within the scope of what can be accomplished at the University of Windsor, unlike an SRAD motor.

To maximize the score even further in the next competition, the team should aim to explore and implement more custom fabrication methods for components such as the body tubing and nose cone of the rocket. This would involve the development of manufacturing processes, with special consideration to ventilation and safe handling of materials, and the integration of even more engineering design components and failure preventative measures to consider.

A final recommendation is to take the final timeline produced by this year’s team into consideration and work to improve on it. This includes more generous time allocations for tasks and frequently following up with individuals on their task progress.

XI. ACKNOWLEDGEMENTS

Our team would like to thank Dr. Defoe for advising our team, the Mechanical, Automotive & Materials Engineering department and the Engineering faculty at the University of Windsor for supporting this project, Mr. Ron Pomerleau from ImaginArtSigns for visuals, and the ESRA with Spaceport America for hosting this year’s 2017 IREC. We would also like to thank our sponsors, particularly all the University of Windsor on campus organizations including the University of Windsor Student Alliance (UWSA), the Alumni Association, Centreline, Kitchen Rescue, Professional Engineers Ontario (PEO), Victoria Steel Corporation, Romano’s Italian Meats & Deli, the University of Windsor Student Life Enhancement Fund, the Engineering Student Society, as well as the Engineering Student Fund (ESF). A special thank you goes out to the University of Windsor technicians which supported the team throughout the execution of this project, notably Andy, Bruce, Dave, Dean, Mark, Matt, Frank, Bill, and Ram, as well as our departmental secretary Angela. The team would like to thank graduate student Sichang Xu for aid in the CFD simulation and post-analysis. Finally, we would also like to thank our friends and family for supporting the team in our fundraising efforts as well as the team members that are not able to join us at the 2017 IREC for their work in this project.

REFERENCES

[1] "SA Cup Documents and Forms - IREC Design, Test, & Evaluation Guide." ESRA, 2017.

[2] "SA Cup Documents and Forms - IREC Rules & Requirements Document." ESRA, pp. 1–25, 2017.

[3] "Misc. Hardware." Canadian Rocket Store.

[4] G. (Tripoli M. Stroick, "Rocket Design," no. February. pp. 1–30, 2010.

[5] "G-10 Fiberglass Epoxy Laminate Sheet," *MatWeb - Material Property Data*. .

[6] G. A. Crowell Sr., "The Descriptive Geometry of Nose Cones," 1996.

[7] G. (Tripoli M. Stroick, "Nose Cone & Fin Optimization," no. January, pp. 1–48, 2011.

[8] N. Mastrocola, "Effect of Number of Fins on the Drag of a Pointed Body of Revolution at Low Supersonic Velocities," NACA Research Memorandum, Langley Field, 1947.

[9] D. C. Cheatham and M. C. Kurbjun, "Transonic Drag Characteristics of a Wing-Body Combination Showing the Effect of a Large Wing Fillet," NACA, Washington, 1948.

[10] E. C. Sanders Jr., "Damping in Roll of Models with 45°, 60°, and 70° Delta Wings Determined at High Subsonic, Transonic, and Supersonic Speeds with Rocket-Powered Models," NACA Research Memorandum, Washington, 1952.

[11] C. Tola and M. Nikbay, "Investigation of the Effect of Thickness, Taper Ratio and nd aspect ratio on fin flutter velocity of a model rocket using response surface method," in *Recent Advances in Space Technologies (RAST)*, 2015.

[12] C. Hoult, "Rocket Science and Engineering Technologies." .

[13] "Elevation and Speed of Sound." .

[14] T. Van Milligan, "Drag of Launch Lugs, Rail Buttons, and Launch Guides." 2017.

[15] "Eggtimer TRS Documentation." Eggtimer Rocketry, 2015.

[16] "Eggtimer Quantum Documentation." Eggtimer Rocketry, 2016.

[17] V. Knowles, "Altimeter Port Sizing." Vern's Rocketry.

[18] "Adept Rocketry - Information on Static Ports," 2012. .

[19] "Technical Guide Kevlar Aramid Fiber," DuPont, 2011.

[20] D. F. Wolf, "Parachute Materials and Stress Analysis," *3rd International Planetart Probe Workshop*. pp. 1–62, 2005.

[21] "48" Heavy Duty Spherachute." Spherachutes.

[22] "SkyAngle CERT-3 Series." The b2 Rocketry Company.

[23] "ASTM D638-14 Standard Test Method for Tensile Properties of Plastics." ASTM

International, West Conshohocken, PA, 2014.

[24] "ASTM D2344/D2344M-16 Standard Test Method for Short-Beam Strength of Polymer Matrix Composite Materials and Their Laminates." ASTM International, West Conshohocken, PA, 2016.

[25] "ANSYS Fluent." ANSYS, Canonsburg, PA.

[26] J. Chartres, "Nanosatellite Launch Adapter System (NLAS)," *Ames Engineering Directorate, NASA*, 2015. .

[27] A. J. Cengel, Yunus A., Ghajar, *Heat and Mass Transfer - Fundamentals & Applications*, 5th ed. New York: McGraw-Hill Education, 2015.

[28] "Simulator Data." ThrustCurve.

[29] S. F. Hoerner, *Fluid-Dynamic Drag*, 2nd ed. Midland Park, NJ: Dr.-Ing. S. F. Hoerner, 1965.

APPENDIX A: MISION CONCEPT OF OPERATIONS OF *THE AMBASSADOR*

The Fig. 4 and Table 2 overviews the phases that *The Ambassador* will undergo during flight. Seven phases of flight are identified in the table, with one preliminary flight phase highlighted as well. In the table, mission phases are identified with the responsible subsystem elaborated, nominal operation of all subsystems listed, and phase transitions highlighted. The mission phases elaborated are later used to help organize failure modes identified in the Risk Assessment Appendix.

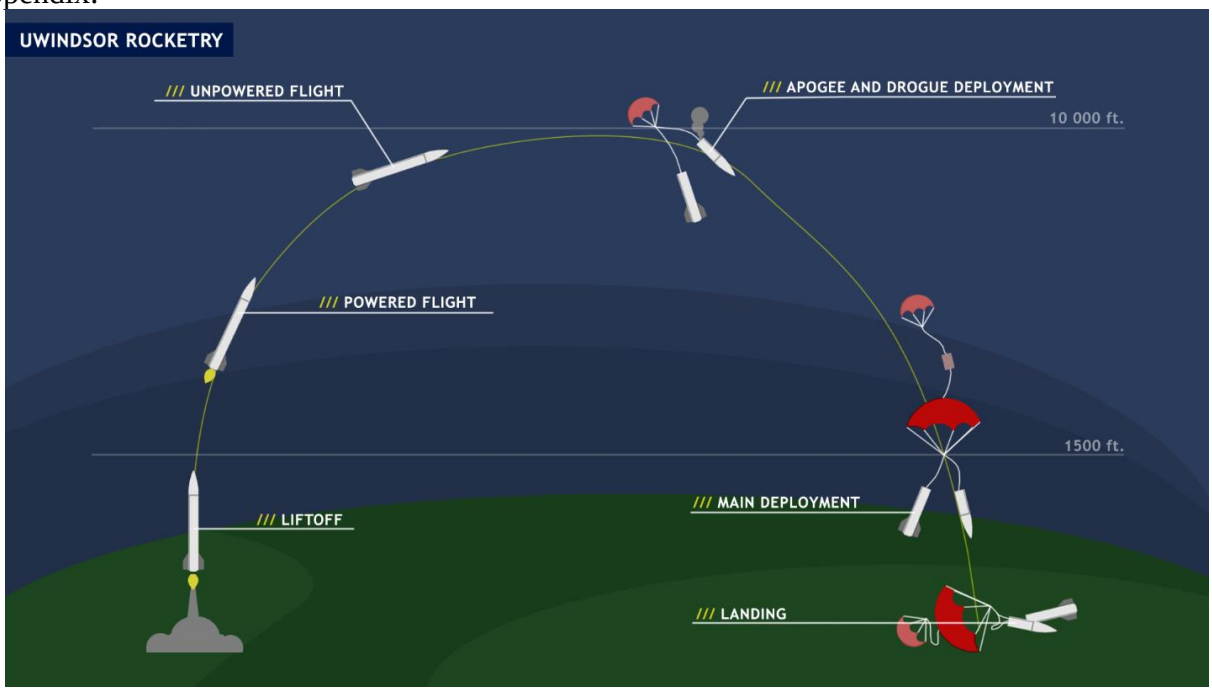

Figure 15: Nominal phases of flight of The Ambassador

Table 11. Mission Concept of Operations Overview of The Ambassador

Phase Number	Phase Title	Phase Description & Nominal Operation of Related Subsystems
0	Vehicle Preparation and Launch Rail Guide Load	Before launching, the main separated vehicle components are assembled and loaded onto the guide rails. This is all done in accordance with the flight checklists included in the Assembly, Preflight, and Launch Checklists Appendix. This is a prerequisite phase of flight and it is required to follow pre-established assembly, preflight, and launch checklists to ensure safe setup and flight. The vehicle has no functionality in this stage the subsystems are deactivated for the user's safety As indicated in the flight checklist, the motor is mounted in the rear of the rocket once the payload, avionics and recovery systems are secured, the tubes are fastened with the screws in the tee-nut connections and the shear pins are installed. The motor's preflight preparation takes place at the launch site. Details of the M1845's

Phase Number	Phase Title	Phase Description & Nominal Operation of Related Subsystems
		motor assembly of the motor itself is included in Fig. 13 in the Key Vehicle Subcomponent Engineering Drawings Appendix. The rocket is carried to the launch site and is loaded onto the ESRA provided launch rail guides (18 ft (5.5 m) long, 1.5 in by 1.5 in (38.1 mm by 38.1 mm) rails) as detailed in the IREC *Design, Test, & Evaluation Guide*[1] in section 8.1. Next, the launch angle of the rail guide is set to 84° ± 1° (weather depending). After the vehicle is mounted onto the guide rails, an igniter is connected to the deactivated ignition system cables provided by the ESRA at the launch area. The igniter is inserted into the nozzle and secured against the motor's smoke charge. Finally, the avionics for the flight computer and recovery systems are armed by turning three switches as further explained in section of this report.
1	Ignition	The ignition phase begins after the vehicle is mounted onto the rail guide, the avionics are armed, and any spectator/participant clears the launch site and principal recovery area[1]. The Safety Monitor activates or arms the starter lines supplying power from the launch controller to the igniter. Once all systems are ready, the safety monitor announces a countdown before sending a signal to the black powder smoke igniter to start the motor. The main subsystem responsible for this phase is the propulsion system, as this phase relates solely to the ignition of the motor propellant. This phase is terminated once the propellant ignites and begins to burn.
2	Liftoff	Liftoff occurs when the rocket first starts to move up the launch rail following the ignition of the motor. The end of this stage is signaled by the exit from the rail. The dominant subsystem operating during this phase is the propulsion system During nominal operation, the solid propellant grain will ignite evenly and carry the rocket up the rail. The motor is an Aerotech M1845NT-P providing a total impulse of 1867.5 lbf-s (8307 N-s) over a period of 4.4 seconds. Its propellant mass is 8.316 lbm (3772 g) and after ignition, it's special *Blue Thunder* propellant releases a trailing pale blue smoke plume. Nominally, this rocket motor produces an average thrust of 421.52 lbf (1875 N). It also produces a liftoff thrust[28] of 505.82 lbf (2250 N). In nominal operation, the rocket must be stable at the end of the guide rail and cannot veer off as soon as it exits. Since the motor powers the rocket to 95 ft/s (29 m/s) at the end of the launch rail, which is below the recommended exit velocity of 100 ft/s (30.5 m/s) [1]. Due to this, additional proof is required to ensure stability as shown in the Flight Appendix. Plots of the rocket's damping ratio, pitch rate and stability have been created. The results from this analysis prove that the rocket is stable. The rail guide buttons as a component of the aero-structure

Phase Number	Phase Title	Phase Description & Nominal Operation of Related Subsystems
		subsystem of the vehicle are also key during operation, as they are used to guide the rocket up the rail towards the sky.
3	Powered Flight	Powered flight begins once the rocket leaves the guide rails and ends once all of the propellant is consumed, otherwise known as the engine burnout. The engine burnout signifies the transition point from powered to unpowered flight. The propulsion system is the main subsystem responsible for accomplishing this paired with the aero-structure subsystem. The propulsion system motor, an Aerotech M1845, has a burn time of 4.4 seconds. The powered flight portion of the rocket accounts for around 24% of the total apogee. This should power the rocket to an apogee of around 650 m (2132.55 ft).The rest of the apogee is gained from the momentum from the powered flight phase in the unpowered ascent of the vehicle. Optimal aero-structure design is key as this phase is a high stress phase. The structure must be strong enough to withstand the subjected forces but also lightweight, ensure. The weight distribution of the rocket has a stability margin between 1 to 2 body calibers.
4	Unpowered Ascent	The unpowered ascent, otherwise known as unpowered flight or coasting, begins after engine burnout. This occurs when the propellant has fully burned from the motor canister, signaling the transition point from powered to unpowered flight. The end of this phase is indicated when the vehicle is no longer ascending and reaches its target AGL apogee. At apogee, the vehicle should tilt horizontally and have a significant velocity reduction. Based on predictive modelling, this will occur at an AGL apogee of approximately 10,000 ft (3,048 m) in nominal operation. The rocket body is carried to apogee by the momentum created during the powered flight phase. The rocket body is designed and all dimensions optimized so that the rocket reaches the target apogee. Thus, the aero-structure and propulsion systems are primarily responsible for the nominal operation of the vehicle during this phase.
5	Initial Deployment Event: Drogue Deployment	The initial deployment event entails the drogue parachute deployment and occurs when the rocket reaches apogee and is no longer ascending. The recovery subsystem is the main system responsible for accomplishing this stage. This phase is triggered by the barometric pressure sensors on the flight computers detecting that the rocket is no longer ascending over a period of 1 second. For nominal operation, the following steps in the initial deployment event will occur in consecutive order: 1. The flight computers detect that the rocket is no longer ascending 2. The flight computer triggers the drogue channel, which fires a charge to the igniter for 2 seconds

Phase Number	Phase Title	Phase Description & Nominal Operation of Related Subsystems
		3. The black powder ejection charge ignites and creates pressure inside the airframe 4. The backup flight computer triggers its drogue channel, which fires a charge to its igniter for 2 seconds, causing its black powder ejection charge to ignite. 5. If problems arise with the charge from the main flight computer, the black powder ignited by the backup flight computer will create pressure inside the airframe. 6. The pressure causes the shear pins to fail, separating the bottom tubing from the coupler. 7. The drogue parachute unfolds 8. The rocket descends at a velocity of about 121.72 ft/s (37.1 m/s). This flight phase ends when the main deployment begins, at an AGL altitude of 1200 ft (365.8 m).
6	Main Deployment Event: Parachute Deployment	The main deployment event entails the main parachute deployment and occurs when the rocket reaches an AGL of 1200 ft (365.8 m). The recovery system is the main system responsible for accomplishing this stage. This phase is triggered by the barometric sensors on the flight computers detecting that the rocket has dropped below 1200 ft (365.8 m) AGL. For nominal operation, the following steps in the main deployment event will occur in consecutive order: 1. The flight computers detect that the rocket has dropped below 1200ft (365.8 m) 2. The flight computer triggers the main channel, which fires a charge to the igniter for 2 seconds 3. The black powder ejection charge ignites and creates pressure inside the airframe 4. The backup flight computer triggers its main channel, which fires a charge to its igniter for 2 seconds, causing its black powder ejection charge to ignite. 5. If problems arise with the charge from the main flight computer, the black powder ignited by the backup flight computer will create pressure inside the airframe. 6. The pressure causes the shear pins to fail, separating the nose cone from the upper tubing. 7. The main parachute unfolds 8. The rocket descends at a velocity of about 27.3 ft/ (8.3 m/s). This flight phase ends when the vehicle lands.
7	Landing & Safe Retrieval	Landing will occur when the vehicle has descended to the ground and is no longer in motion. At landing, the recovery subsystem will nominally operate as follows: 1. The flight computer detects that the rocket is below 30 ft (9.144 m) for over 5 seconds

Phase Number	Phase Title	Phase Description & Nominal Operation of Related Subsystems
		2. The flight computer continues to send altitude and GPS coordinates to Eggfinder LCD Once this occurs, the group will locate the vehicle and safely retrieve the motionless vehicle. The collection of the separated components will indicate the completion of this phase as well as the end of the complete flight cycle.

APPENDIX B: HAZARD ANALYSIS APPENDIX

The following table aims to address all aspects of the design which pose potential hazards to operating personnel, including, notably, hazardous material handling, transportation and storage procedures of propellants. Mitigation approaches, by process and/or design, are also defined for each hazard identified.

Table 12. Hazard Analysis Overview

Hazard Analysis Scenario	Identified Risks	Mitigation Approach	Risk Assessment
Fiberglass cutting and sanding	- Fiberglass inhalation - Fiberglass abrasion of the skin	- Use appropriate personal protective equipment (PPE). Usage of gloves and safety mask during material manipulation	Low
Black powder storage	- Flammable - Static electricity - Impact	- Store in a secure, cool and dry place, away from flammable substances and any sources of ignition with limited access	Low
Black powder transportation & handling	- Impact, friction, static cause it to ignite - Adverse effects upon digestion	- Use appropriate personal protective equipment (PPE). Usage of gloves and safety mask during material manipulation - Clean up spills carefully with non-sparking & non-static producing tools - Black powder is stored in inert isolated controlled environment, away from the igniters and any other source of heat or flammable substance, during transportation - In its insulated storage container, the black powder will not be left unattended, in a hot vehicle, or in direct sunlight	Low
Black powder ejection charge testing	- Detonation produces hazardous overpressures and fragments	- Be well away from charge during ignition - Eggtimer suggests 10ft between anyone and the rocket when testing. - No personnel	Medium

Hazard Analysis Scenario	Identified Risks	Mitigation Approach	Risk Assessment
	- Toxic gases can be created - Deflagrating explosive	stands in the direct path that the rocket is expected to take	
Igniter storage	- Potential explosion risk	- Store in inert isolated controlled environment, away from the black powder and any other source of heat or flammable substance	Low
Storage of high power rocket motors	- Potential explosion risk - Propellant poses toxicity risks if ingested or inhaled - Highly flammable substance - Risk of overheating or explosion if not properly stored in an appropriate environment	- This is being mitigated by having the supplier store the motors being used. Company personnel has experience with hazardous material handling and proper motor storage techniques	Low
High power rocket motor transportation and handling	- Potential explosion risk - Propellant poses toxicity risks if ingested or inhaled - Highly flammable substance - Risk of overheating or explosion if not properly stored in an appropriate environment	- This is being mitigated by having the supplier bring the motors directly to the competition. The delivery personnel has experience with hazardous material handling and proper motor storage techniques - Store in a secure, cool and dry place, away from flammable substances and any sources of ignition with limited access	Low
Ignition of high power rocket motors	- Explosion risk - Highly flammable, controlled substance	- Practice ignition process with test launch - Rehearse and be aware of - Follow a launch checklist	Med
Black powder ejection charge	-Detonation produces hazardous	- Be well away from test site during launch	Low

Hazard Analysis Scenario	**Identified Risks**	**Mitigation Approach**	**Risk Assessment**
during drogue and main parachute deployment	overpressures and fragments - Toxic gases can be created - Deflagrating explosive - Black powder charge leads to excessive damage to the rocket or shock, leading to components landing at an accelerated pace	- Use of a redundant system - Use of a pre-flight and launch checklist to ensure that the setup of the electronics is correct	
Safe collection of rocket vehicle components post-launch	- Broken components on the ground of the landing site pose a risk of injury during collection due to sharp edges - Burned ignition after recent launch poses a risk of inhalation	- Use protective gloves during vehicle collection if it has broken in pieces - Wear closed-toed shoes to prevent stepping on broken components - Do not carry any of the components close to your face to avoid inhaling burned ignition remnants	Low

APPENDIX C: RISK ASSESSMENT APPENDIX

The following table aims to address all aspects of the flight which pose potential hazards to operating personnel, including notably hazardous material handling, transportation, and storage procedures of propellants. Mitigation approaches, by process and/or design, are also defined for each hazard identified.

Table 13. Risk Assessment Overview

Phase (as described by the CONOPS)	**Hazard**	**Possible Causes**	**Risk of Mishap and Rationale**	**Mitigation Approach**	**Risk of Injury After Mitigation**
Vehicle Preparation and Launch Guide Rail Load	Rocket is loaded incorrectly onto the guide rail and falls off the rail, onto a team member	- Misalignment of rail buttons to the guide rail - Extreme unbalance of the rocket - Quick and negligent loading of the vehicle onto the rail guides	Low: - Limited degrees of freedom because of the three rail buttons chosen for use	- Practice loading the vehicle on the launch guide rails before launch - Follow a pre-launch checklist	Low
Ignition	Rocket ignition does not occur on ‘FIRE’ and occurs with a delay, as the team approaches the vehicle	- Faulty connection - Ignition connection is not properly set up	Low: - Simple connection process - Short process, so if done wrong initially, can be set up again in a short amount of time	- Ignition setup is practiced beforehand in a test launch - Double check all wiring - Ensure that the igniter is full inserted into the motor and is in contact with the propellant - Secure igniter to the motor retainer to ensure that it does not fall out	Low

Phase (as described by the CONOPS)	**Hazard**	**Possible Causes**	**Risk of Mishap and Rationale**	**Mitigation Approach**	**Risk of Injury After Mitigation**
Liftoff	Pivoting occurs when the first rail button has left the launch rail and rocket begins to rotate or pivot about the remaining rail button, leading to potentially barreling and launch failure	- Poor stability of the rocket - High wind speeds -Low off the rail velocity (fins are not able to stabilize rocket)	Low: -Stability, damping moment, corrective moment, thrust to weight ratio have been verified to ensure stability	- Larger fins so that rocket is stable - High off rail velocity to ensure that fins are able to stabilize rocket	Low
Powered Flight	Fin flutter occurs, causing the rocket to become unstable	- Instability of the fins at the higher speeds - Fins can break	Low: - Fin flutter calculations have been made to ensure that the rocket is not travelling at speeds high enough to induce flutter	- Verify fin assembly to ensure that there is no damage to either the fins or the fin canister assembly - If damage exists, repair this so that the rocket can be flown after the repairs are complete	Low
	Structural failure occurs in the airframe of the vehicle	- Impurities in the airframe causing weak points in the structure - Weak structure	Low: - Fiberglass is being used, and it is able to withstand the body forces	- Inspect material to ensure that no imperfections exist - If imperfections	Low

Phase (as described by the CONOPS)	**Hazard**	**Possible Causes**	**Risk of Mishap and Rationale**	**Mitigation Approach**	**Risk of Injury After Mitigation**
		- Structure is not structurally sound in design	that it is exposed to - Rocket body has been design so it remains within optimal slenderness ratio values - Body is not excessively long, and this prevents rocket body from folding in on itself	exist, take necessary steps to mend - Material used is fiberglass, so structural stability of the material is not a concern -rocket body is appropriately dimensioned, length to diameter ratio is within optimal range (15.6:1)	
Unpowered Ascent	The dual deployment goes off mid-flight	- Electronics failure - Pressure venting failure	Low: - Multiple static pressure ports chosen to evenly distribute the pressure on the	- Using COTS electronics which have been thoroughly tested and include Mach transition immunity through mathematical filtering - Multiple static pressure ports drilled to reduce influence of winds and to ensure undisturbed	Low

Phase (as described by the CONOPS)	**Hazard**	**Possible Causes**	**Risk of Mishap and Rationale**	**Mitigation Approach**	**Risk of Injury After Mitigation**
				access to outside air pressure	
Initial Deployment Event: Drogue Deployment	Black powder is insufficient to separate tubing and coupler	- Ejection charge undersized	Low - Black powder charge is sized with a factor of safety to ensure it separates the body - Backup charge exists	- Ground testing to size black powder - 0.2 grams are added to backup ejection charge to ensure deployment	Low
	Parachute tangles or gets stuck and does not properly deploy, leading to the vehicle to land at an accelerated rate	- Parachute not loaded properly - Parachute failure - Parachute is incorrectly sized for use - Recovery harness failure or entanglement	Medium - Shroud lines still present a risk of getting entangled - Inside surfaces of rocket contain weld nuts	- Parachute must be folded properly so that the lines don't interfere with each other - Parachute has only 4 shroud lines so there is less chance of tangle	Low
	Drogue parachute does not deploy, causing the rocket to accelerate downwards at	- Failure of electronics e.g. from using old batteries or not turning on all electronic components	Medium - Batteries will be fully charged before the launch - Backup charges exist in case main	- Wiring is to standards specified by IREC - Electronics are pretested - New batteries that checked to be	Low

Phase (as described by the CONOPS)	Hazard	Possible Causes	Risk of Mishap and Rationale	Mitigation Approach	Risk of Injury After Mitigation
	uncontrollable speeds	- Shear pins do not fail as intended - Faulty wiring - Improper loading of the parachute - Parachute entanglement	charges do not separate the rocket - Wiring is up to IREC standards - If failure occurs, could result in possible harm to others or property	fully charged are used - Follow a pre-launch checklist during setup - There is a completely independent backup deployment that also occurs with a slightly larger charge -TRS has a separate battery for deployment - Battery terminal connections and wires inspected prior to launch	
	Parachute tears during deployment, leading to the vehicle at unsafe speeds	- Parachute can shoot out and not open up - Rocket will hit ground at high velocities and lead to damage - A parachute that is too small will also lead to body damage - Improperly attached harness can mean that the	Medium - Parachute needs to be folded properly - Cannot be too compact - Shroud lines cannot be entangled - Connection to harness is strong enough to	- Parachute will be folded accurately and placed in the body in a way that it avoids any interference with fasteners on the inside body - This will prevent shroud lines	Low

Phase (as described by the CONOPS)	Hazard	Possible Causes	Risk of Mishap and Rationale	Mitigation Approach	Risk of Injury After Mitigation
		parachute separates from the body	withstand opening shocks	will be untangled before folding parachute - Connections to the harness will be double checked to ensure that everything is properly secure	
	During ejection charge, the parachute is not fully protected by the Nomex heat-protector blanket and burns from exposure, leading to the vehicle to descend at an accelerated rate	- Improper loading of the parachute - Nomex - Parachute entanglement	Low: - Thermally stable, flame retardant material is used - Parachute loading is practiced	- Practice folding the parachute for proper installation and reduction of shroud line entanglement	Low
	Recovery harness fails, sending the separated components to fall at accelerated rates	- Improper loading and attachment of the harness - Nomex harness protector is forgotten in the preflight assembly - Harness breaks	Low: - Recovery harness is selected from	- Preflight assembly checklist is used - Ensure harness attachment and knots used are sturdy	Low

Phase (as described by the CONOPS)	**Hazard**	**Possible Causes**	**Risk of Mishap and Rationale**	**Mitigation Approach**	**Risk of Injury After Mitigation**
		- Harness is poorly knotted			
Main Deployment Event: Parachute Deployment	Black powder is insufficient to separate tubing and nose cone	- Ejection charge undersized	Low - Black powder charge is sized with a factor of safety to ensure it separates the body - Backup charge exists	- Ground testing to size black powder - 0.2 grams are added to backup ejection charge to ensure deployment	Low
	Main parachute does not deploy, leading to the vehicle to descend at an accelerated rate	- Failure of electronics e.g. from using old batteries or not turning on all electronic components - Shear pins do not fail as intended - Faulty wiring - Improper loading of the parachute - Parachute entanglement	Medium - Batteries will be fully charged before the launch - Backup charges exist in case main charges do not separate the rocket - Wiring is up to IREC standards - If failure occurs, could result in possible harm to others or property	- Wiring is to standards specified by IREC - Electronics are pretested - New batteries that checked to be fully charged are used - Follow a pre-launch checklist during setup - There is a completely independent backup deployment that also occurs with a slightly larger charge	Low

Phase (as described by the CONOPS)	Hazard	Possible Causes	Risk of Mishap and Rationale	Mitigation Approach	Risk of Injury After Mitigation
				-TRS has a separate battery for deployment - Battery terminal connections and wires inspected prior to launch	
	Parachute tangles or gets stuck and does not properly deploy, leading to the vehicle to descend at an accelerated rate	- Parachute not loaded properly - Parachute failure - Parachute is incorrectly sized for use - Recovery harness failure or entanglement	Low - Not many components inside rocket to interfere with parachute loading - MATLAB used to size parachute so that descent velocity is within acceptable range - Harness is secured properly, and shroud lines are stowed and folded safely	- Perform ground test to ensure that parachute deploys properly - Ensure that parachute is not damaged in any way pre-flight - Test the connection between the parachutes and the harnesses - Untangle shroud lines before folding to reduce risk of entanglement	
	Main parachute tears during deployment, leading to the	- Parachute not loaded properly - Parachute failure	Low - Drogue slows down rocket to a manageable	- Flight checklist in place to ensure that deployment	Low

Phase (as described by the CONOPS)	Hazard	Possible Causes	Risk of Mishap and Rationale	Mitigation Approach	Risk of Injury After Mitigation
	vehicle to descend at an accelerated rate		speed before it is deployed	charge for drogue chute is set up correctly, along with the backup charge in order to make sure that the drogue deploys and slows down the rocket	
	During ejection charge, the parachute is not fully protected by the Nomex heat-protector blanket and burns from exposure, leading to the vehicle to descend at an accelerated rate	- The parachute protector is improperly folded around the parachute - Nomex parachute protector is forgotten in the assembly	Low: - Thermally stable, flame retardant material is used - Parachute loading is practiced	- The parachute will be placed inside the body in such a way that there is no direct contact between the parachute and the black powder canisters	Low
	Main parachute deploys earlier than anticipated, drifts away from the launch zone to civilian area or highway	- Rocket separates prior to apogee - failure of electronics	Medium - If failure, could cause accident or injury to civilians - Ground testing done prior to launch	- Ground test ensuring done to ensure proper deployment charge and test accuracy of calculations	Low

Phase (as described by the CONOPS)	**Hazard**	**Possible Causes**	**Risk of Mishap and Rationale**	**Mitigation Approach**	**Risk of Injury After Mitigation**
				- Shear pins used instead of friction fit - COTS avionics used with integrated Mach immunity and many tests done by manufacturer to ensure parachutes are deployed at correct altitude	
Landing & Safe Retrieval	Rocket has a high impact velocity and lands dangerously	- Parachute failure - Parachute is incorrectly sized for use - Shock cord failure - harness failure	Medium - MATLAB used to size parachute so that descent velocity is within acceptable range - Connection to harness is strong enough to withstand opening shocks	- Ensure that parachute is not damaged in any way - Connections will be double checked to ensure that they are secure	Low
	Rocket lands in a tree or on a structure, breaking and sending pieces	- Landing on an obstruction - Early deployment causing the vehicle to drift	Low - Launch zone is in the middle of the desert, there are very few	- Use of a longer shock cord	Low

Phase (as described by the CONOPS)	**Hazard**	**Possible Causes**	**Risk of Mishap and Rationale**	**Mitigation Approach**	**Risk of Injury After Mitigation**
	of the rocket flying		structures in the		

APPENDIX D: ASSEMBLY CHECKLIST

ASSEMBLY CHECKLIST

Payload and Payload Bay

- ❑ Insert mass into the payload bay in the nose cone.
- ❑ Secure payload.

Nose cone

- ❑ Secure nose cone to the payload.
- ❑ Insert shoulder into nose cone, align the correct markings and holes. Ensure a flush fitting.
- ❑ Insert and tighten weld nuts to connect the shoulder to the nose cone
- ❑ Ensure all fittings are secured; making sure that all screws/nuts/bolts are completely attached and tightened.

Top Body

- ❑ Make sure all parachute lines and shock cords are undamaged, looking particularly for frayed, burnt and/or rotted fibres. Verify that the shroud lines are all of equal length.
- ❑ Attach parachute to shock cord. Attach parachute to the line at approximately ⅓ the length (connection area to be pre-marked).
- ❑ Attach shock cord to U-Bolt on the bottom of payload bay bulkhead
- ❑ Carefully fold the parachute and shock cord and place in the top body. Ensure that the safety harness Nomex protectors and Nomex parachute heat protector blanket are installed in the assembly. Zip tie the Nomex blanket to the shock cord to ensure it does not slide.
- ❑ Verify 'burrito' parachute folding.
- ❑ Insert nose cone and shoulder into the top body.
- ❑ Insert shear pins to ensure that top body is secure and does not move.

Electronics

- ❑ Setup data acquisition electronics (Arduino & Pi)
    - ❑ Check the charge of the batteries
    - ❑ Charge batteries that are not fully charged
    - ❑ Verify batteries are zip tied and all electronics are well fastened to sled
    - ❑ Set up recovery electronics
    - ❑ Check the charge of the batteries
    - ❑ Record voltage of batteries here:
      TRS Main _____V, TRS Deployment _____V, Quantum _____V
    - ❑ Charge batteries that are not fully charged
    - ❑ Ensure batteries are fully connected in avionics bay
    - ❑ Inspect bay for frayed or broken wires
    - ❑ Conduct tug test on all wires
    - ❑ Tighten all bolts and screws
    - ❑ Verify that avionics are well secured to sled

- ❑ Verify that batteries are zip tied to sled
- ❑ Verify that threaded rods are all secured to sled

❑ Set up the ejection charges

- ❑ Measure FFFFg black powder required for drogue and main deployment
- ❑ Close/seal black powder containers
- ❑ Label charges Main Primary (MM), Main Backup (MB), Drogue Primary (DM), Drogue Backup (DB)
  Record amounts here:
  Main Primary _____g, Main Backup _____g,
  Drogue Primary _____g, Drogue Backup _____g

Bottom Body

- ❑ Secure thrust ring into place with nuts
- ❑ Build motor hardware set as per instructions provided by the manufacturer and install the motor hardware set into the lower body tubing section.
- ❑ Load the motor into the motor mount.
- ❑ Bolt motor retainer into place.
- ❑ Lock retaining ring in place, ensure that the motor does not slide out.
- ❑ Make sure all parachute lines and shock cords are undamaged, looking particularly for frayed, burnt and/or rotted fibres. Verify that the shroud lines are all of equal length.
- ❑ Attach shock cord to drogue.
- ❑ Attach shock cord to eye bolt on the head of the motor hardware set.
- ❑ Attack shock cord to backup U-Bolt on the top centering ring.
- ❑ Carefully fold the parachute and shock cord and place in the top body. Ensure that the safety harness Nomex protectors and Nomex parachute heat protector blanket are installed in the assembly. Zip tie the Nomex blanket to the shock cord to ensure it does not slide.
- ❑ Verify ‘burrito’ parachute folding.
- ❑ Daisy chain the shock cord at the lower body section connection.
- ❑ Load top body assembly into bottom body, aligning holes and markings for coupler and venting.
- ❑ Insert shear pins to ensure that bottom body is secured to the upper assembly and does not move.

PREFLIGHT CHECKLIST

Electronics

- ❑ Calibrate data acquisition electronics
    - ❑ Check the charge of the batteries
    - ❑ Charge batteries that are not fully charged
    - ❑ Orient the sled with respect to magnetic north, and document orientation
    - ❑ Connect batteries to microcontroller and raspberry pi systems
    - ❑ Place avionics bay in 6 standing positions for 30 seconds each, at different orientations to calibrate gyroscope and accelerometer
        - ❑ 1 ❑ 2 ❑ 3 ❑ 4 ❑ 5 ❑ 6
    - ❑ Wave in "figure 8" motions for 10 seconds to calibrate magnetomer
- ❑ Set up recovery electronics
    - ❑ Check the charge of the batteries
    - ❑ Charge batteries that are not fully charged
    - ❑ Ensure batteries are fully connected in avionics bay
    - ❑ Confirm that all avionics are unpowered/all switches are turned off
    - ❑ Screw wires from igniters and flight computers into their respective terminal blocks
    - ❑ Perform tug test on igniter wires
    - ❑ Turn on switches to power Eggtimer TRS
    - ❑ Turn on Eggfinder LCD
    - ❑ Check continuity of main and drogue channels
    - ❑ Confirm all flight settings are correct.
    - ❑ Turn off switches to power Eggtimer TRS
    - ❑ Turn on switch to power Eggtimer Quantum
    - ❑ Connect to Eggtimer Quantum via Wifi
    - ❑ Check continuity of main and drogue channels
    - ❑ Confirm all flight settings are correct.
    - ❑ Turn off switch to power Eggtimer Quantum.
    - ❑ Ensure batteries are fully connected in avionics bay
    - ❑ Inspect bay for frayed or broken wires
    - ❑ Conduct tug test on all wires
    - ❑ Tighten all bolts and screws
    - ❑ Verify that avionics are well secured to sled
    - ❑ Verify that batteries are zip tied to sled
    - ❑ Verify that threaded rods are all secured to sled
    - ❑ Verify that all switches are in off position (110)
- ❑ Secure avionics bay
    - ❑ Load avionics bay into the body coupler
    - ❑ Add putty to threaded rods

- ❑ Secure the top bulkhead onto the coupler using wing nuts
- ❑ Ensure that the wing nuts are fully tightened

❑ Set up the ejection charges

- ❑ Verify black powder charge sizes.
- ❑ Record amounts here:

  Main Primary _____g, Main Backup _____g,

  Drogue Primary _____g, Drogue Backup _____g

- ❑ Insert igniter into charge well
- ❑ Pour black powder into charge well
- ❑ Insert insulating material into charge well
- ❑ Pack material with dowel
- ❑ Seal charge well with tape

❑ Secure avionics bay to the rest of the rocket

- ❑ Attach shock cords from main and drogue parachutes to the U-Bolts
- ❑ Ensure that the connection is secure
- ❑ Load coupler into top body and secure using bolts
- ❑ Load lower body onto coupler and secure using shear pins

Inspection

- ❑ Inspect the vehicle for damage in the nose cone, air frame, & fins.
- ❑ Check that the nose cone snuggly fits into the airframe.
- ❑ Verify that the fins are secured. Wiggle them slightly to check.
- ❑ Verify that the motor mount is secured with no loose parts.
- ❑ Ensure that the guide rail buttons are aligned.

FLIGHT CHECKLIST

- ❑ Load the vehicle on the guide rails.
- ❑ Ensure that the guide rail has a launch elevation angle of 84° ± 1° (may be reduced to 70° based on weather) based on subsection 8.1 of the 2017 IREC Design, Test, & Evaluation Guide1.
- ❑ Arm electronics by turning all three switches counterclockwise from 110 to 220 position (off to on).
- ❑ Set up the igniter. Install the igniter and ensure that it touches the black smoke charge.
- ❑ Leave the launch site and go to a safe distance.
- ❑ Verify flight settings on the Eggfinder LCD receiver and then select 'Start a Flight'
- ❑ Check status on the Eggfinder LCD receiver.
- ❑ Connect to Eggtimer Quantum via Wifi.
- ❑ Connect to 192.168.4.1 via phone browser – preferably Firefox.
- ❑ Verify flight settings and arm the Quantum.
- ❑ Press the launch button and watch the rocket ascent to the sky.

APPENDIX E: ENGINEERING DRAWINGS

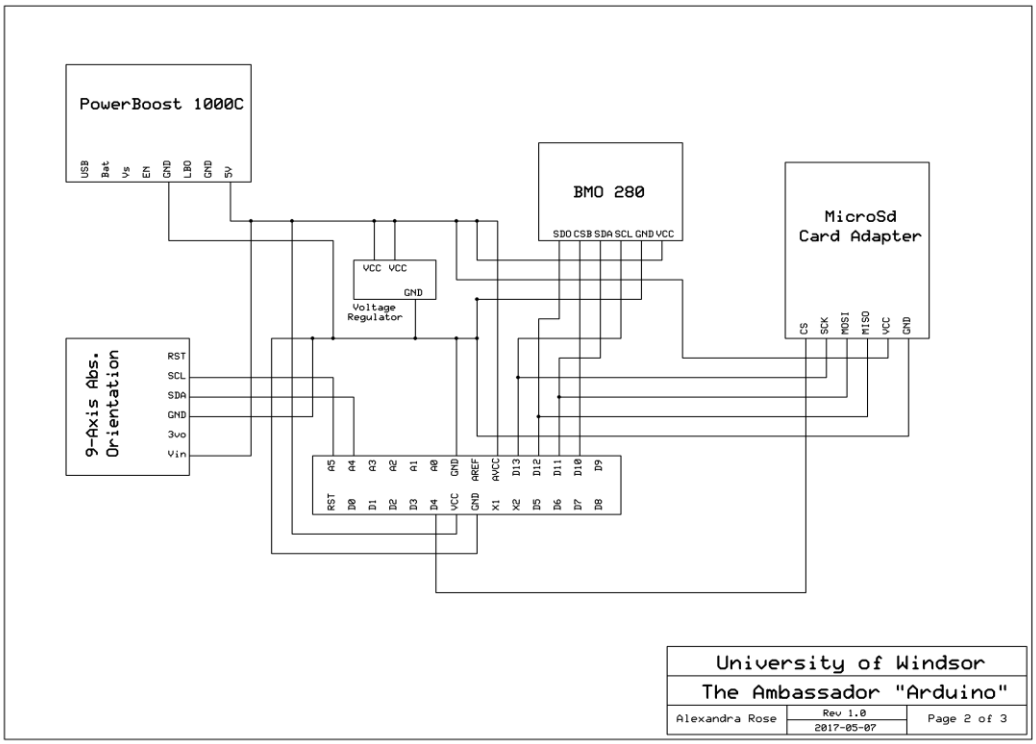

Figure 16: Wiring Diagram of the Arduino Avionics Component of The Ambassador

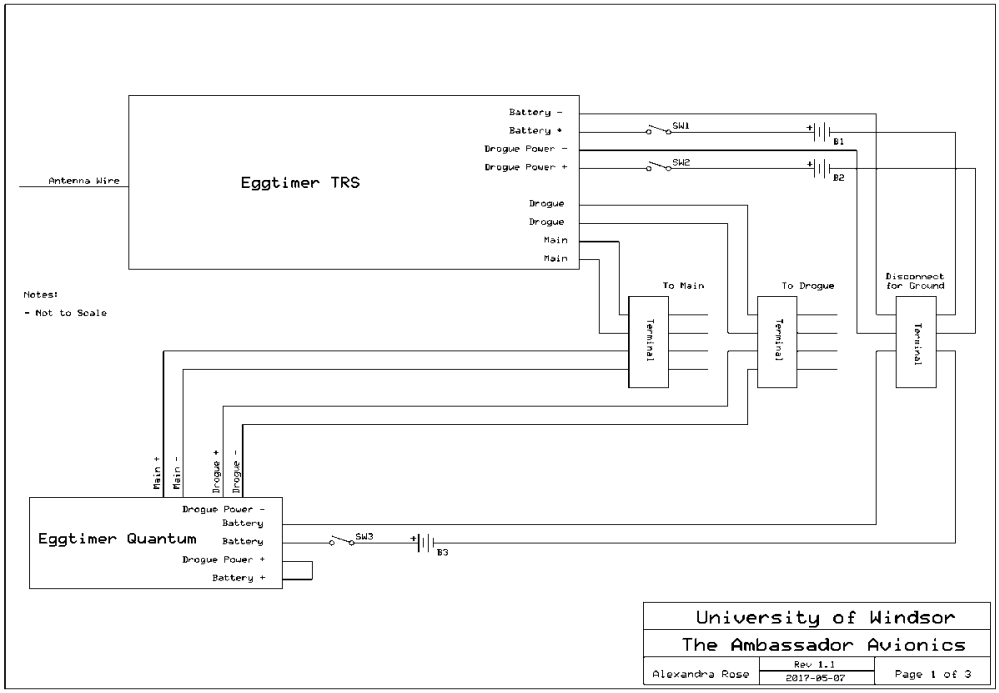

Figure 17: Custom Electronics - Wiring Diagram of the Eggtimer TRS and Quantum Avionics Solution of The Ambassador

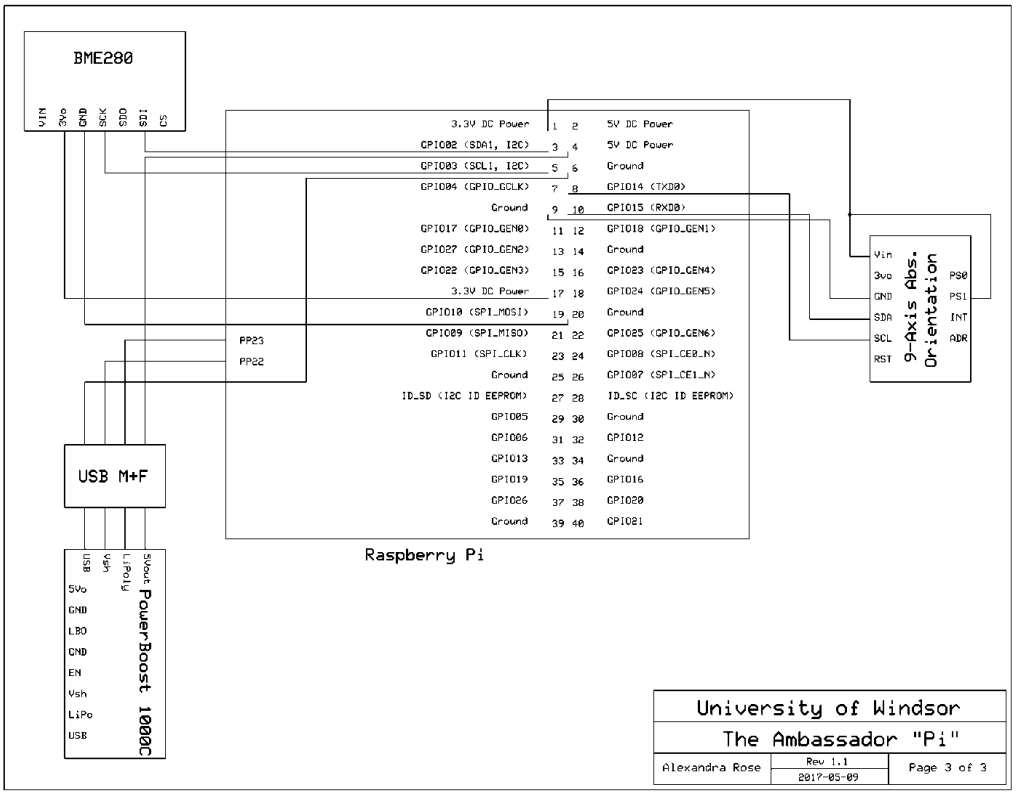

Figure 18: Custom Electronics - Wiring Diagram of the Raspberry Pi Avionics Component

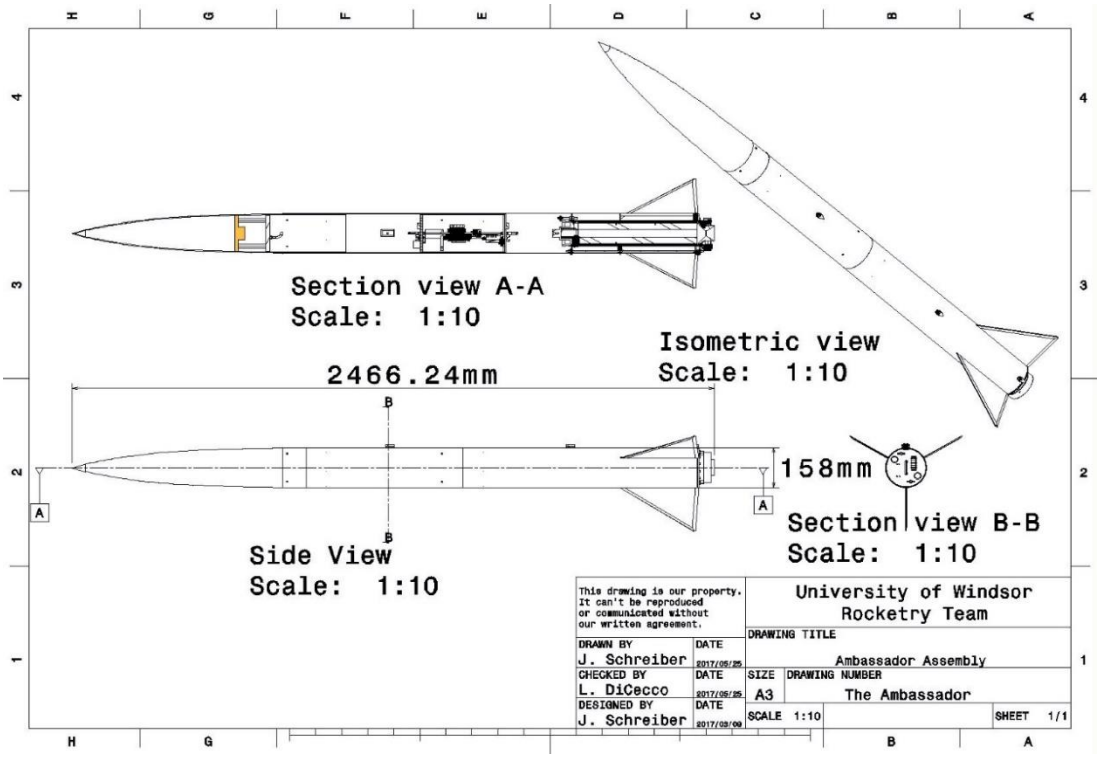

Figure 19: The Ambassador - Assembled CATIA Drawing

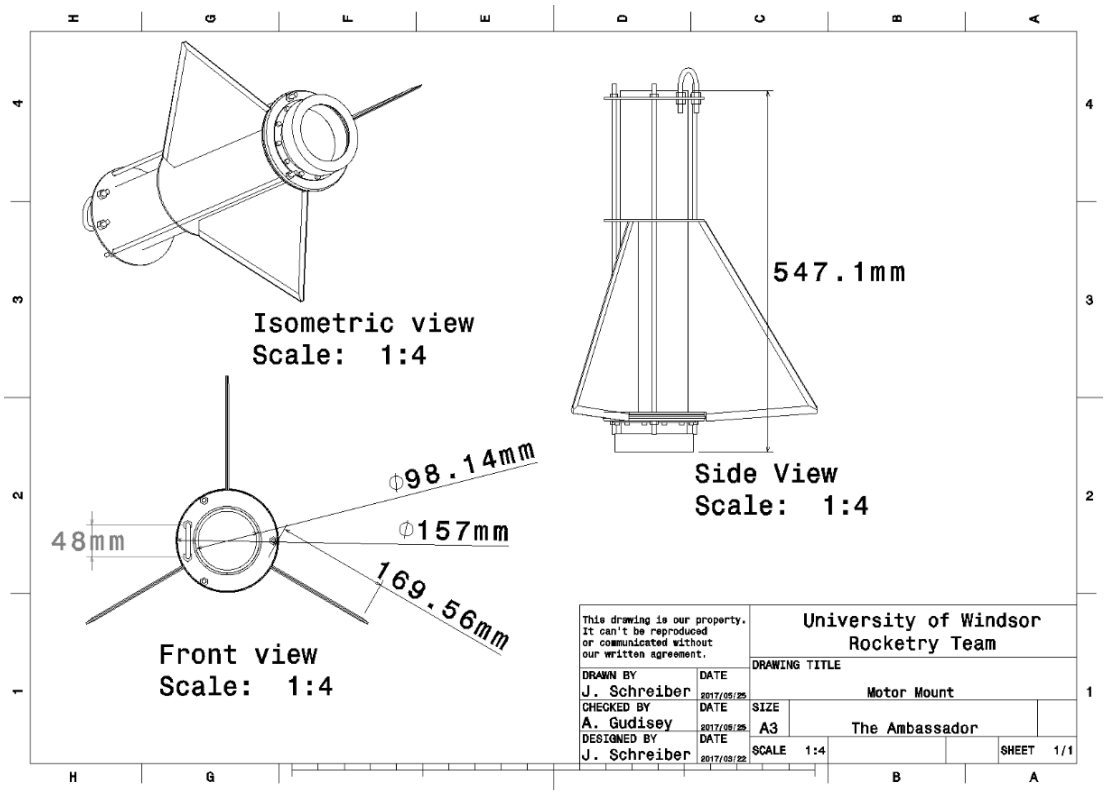

Figure 20: Motor Mount and Fin Assembly Drawing

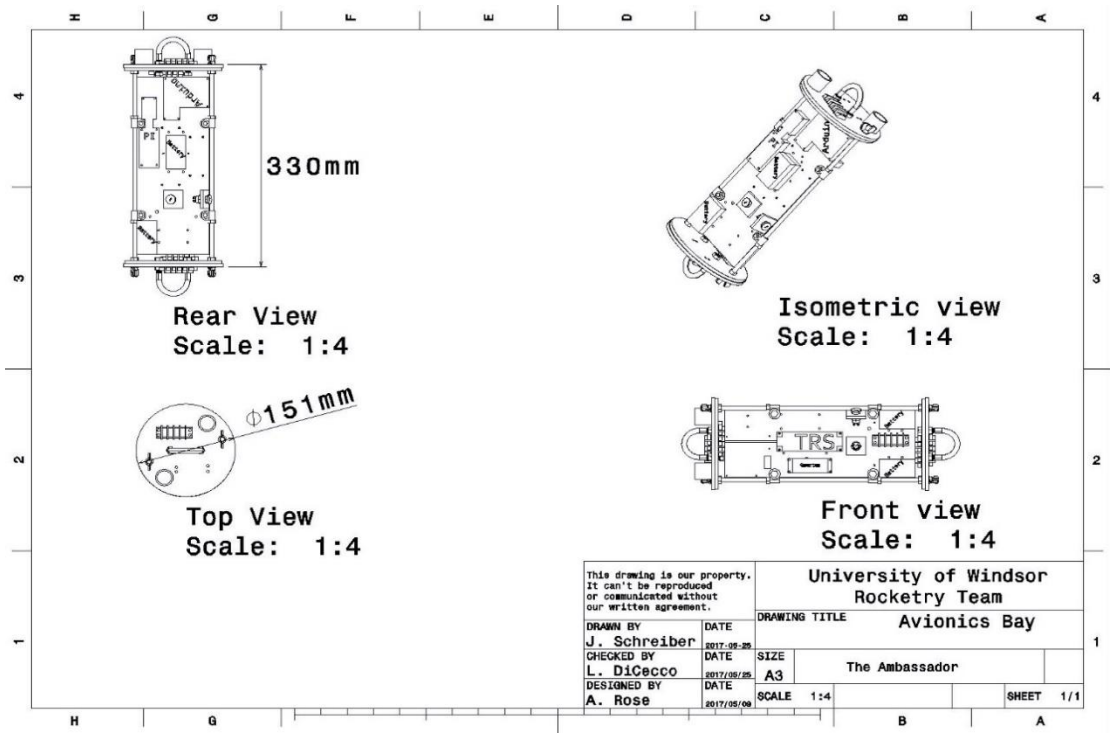

Figure 21: Avionics Bay Overview Drawing

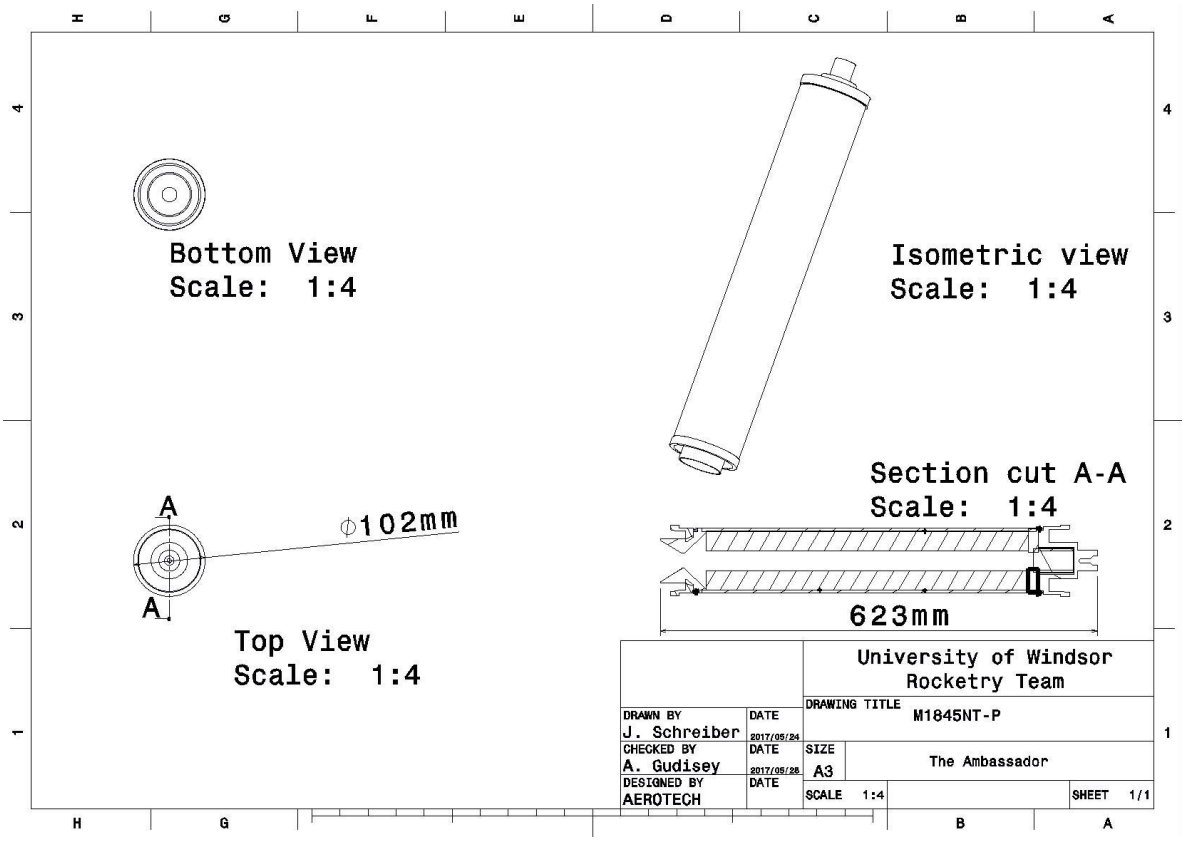

Figure 22: M1845NT-P Motor [3]

APPENDIX F: AVIONICS SELECTION ANALYSIS

The following table identifies the various combinations of consumer products available which would fulfil the avionics requirements. The weight and cost points are derived by dividing the weight or cost of that option by the respective weight or cost of the heaviest or most expensive option and then dividing that number by 5. The technical complexity was determined by appointing 3 points to options which required a HAM radio license, 2 points to options which required assembly, and 1 point for every component required to fulfil the requirements. The cost and weight are calculated with the assumption that there is a redundant system being implemented as well.

Table 14. Avionics Cost Analysis

Package	Cost (USD $)	Cost Points (0-5)	Weight (g)	Weight Points (0-5)	Ham-Radio (Y/N)	Tech Complexity (0-7)	Score (0-17)	Score w/o Tech Complexity (0-10)
TeleGPS Chute Release	842.00	4	58.4	3	Y	5	12	7
Big Red Bee 70cm	520.00	2	50	2	Y	4	8	4
Altus Metrum	798.00	4	40.26	2	Y	4	10	6
BRB900 Chute Release	876.00	5	84.02	4	N	2	11	9
TeleGPS Stratologger	736.41	4	45.92	2	Y	5	11	6
BRB900 Stratologger	770.41	4	71.54	3	N	2	9	7
Eggtimer TRS	247.00	1	50	2	N	3	6	3
Eggtimer TRS Eggtimer Quantum	197.00	1	35	1	N	4	6	2
EggTimer EggFinder	235.00	1	80	4	N	4	9	5
BRB900 EggTimer	384.00	2	90	5	N	4	11	7
TeleGPS EggTimer	659.00	3	64.38	3	Y	7	13	6
Stratologger EggFinder	312.41	1	61.54	3	N	4	8	4

APPENDIX G: ROCKET VEHICLE ANALYSIS

I. Centre of Mass

$$X_{cm(R)} = \frac{\sum(X_p + X_{cm(P)})M_P}{M_R} \tag{1}$$

II. Centre of Pressure

$$X_{cp(R)} = \frac{\sum C_{N\alpha(P)} X_{cp(P)}}{\sum C_{N\alpha(P)}} \tag{2}$$

Stability Derivative of Nosecone

$$C_{N\alpha(n)} = 2 \tag{3}$$

$$X_{cp(n)} = \frac{l_n}{2} \tag{4}$$

Stability Derivative of Fins

$$C_{N\alpha(f)} = K_{fb} \frac{4n(\frac{l_s}{d_n})^2}{1+\sqrt{1+(\frac{2l_m}{l_r+l_t})^2}} \tag{5}$$

$$X_{cp(f)} = X_f + \frac{l_m(l_r+2l_t)}{3(l_r+l_t)} + (1/6)(l_r + l_t - \frac{l_r l_t}{l_r+l_t}) \tag{6}$$

III. Static Stability

$$\partial S = \frac{X_{cp(R)} - X_{cm(R)}}{d_b} \tag{7}$$

IV. Viscous Effects

Reynolds Number

$$Re = \frac{\rho V L}{\mu} \tag{8}$$

Critical Reynolds Number

$$R_{crit} = 51(\frac{R_s}{L})^{-1.039} \tag{9}$$

Viscous Friction (Re > 10^4)

$$C_f = 0.032(\frac{R_s}{L})^{0.2} \tag{10}$$

Viscous Friction *(Re < 10^4) & (Re < Rec)*

$$C_f = \frac{1.328}{\sqrt{Re}} \tag{11}$$

Viscous Friction *(Re < 10^4) & (Re > Re_c)*

$$C_f = \frac{0.074}{Re^{(1/5)}} - \frac{B}{Re} \tag{12}$$

V. Pressure Properties

Stagnation Point Pressure Coefficient

$$C_{pT} = (\frac{P_T}{P_\infty} - 1)(\frac{2}{\gamma M^2}) \tag{13}$$

Stagnation Pressure Ratio

$$\frac{P_T}{P_\infty} = (1 + \frac{\gamma - 1}{2} M^2)^{\frac{\gamma}{\gamma - 1}} \tag{14}$$

VI. Coefficients of Drag

Forebody Drag Coefficient

$$C_{D(fb)} = (1 + \frac{60}{(l_{TR}/d_b)^3} + 0.0025\frac{l_b}{d_b})(2.7\frac{l_n}{d_b} + 4\frac{l_b}{d_b} + 2(1 - \frac{d_d}{d_b})\frac{l_c}{d_b})C_{f(fb)} \tag{15}$$

Base Drag Coefficient

$$C_{D(b)} = 0.02\frac{(d_d/d_b)^3}{\sqrt{C_{D(fb)}}} \tag{16}$$

Fin Drag Coefficient

$$C_{D(f)} = 2C_{f(f)}(1 + 2\frac{T_f}{l_m})\frac{4nA_{fp}}{\pi d_f^2} \tag{17}$$

Interference Drag Coefficient

$$C_{D(i)} = 2C_{f(f)}(1 + 2\frac{T_f}{l_m})\frac{4n(A_{fp} - A_{fe})}{\pi d_f^2}$$

Total Drag Coefficient

$$C_D = C_{D(fb)} + C_{D(b)} + C_{D(f)} + C_{D(i)} \tag{18}$$

VII. Parasite Drag [29]

Rail Button Drag Coeffcient

$$C_{D(rb)} = 0.8\eta_{airfoil}\frac{A_{rb}C_{pT}}{A_{ref}} \tag{19}$$

Vent Hole Drag Coeffcient

$$C_{D(vh)} = 0.0041\frac{A_{vh}C_{pT}}{A_{ref}} \tag{20}$$

Shear Pin Drag Coeffcient

$$C_{D(sp)} = 0.32\frac{A_{sp}C_{pT}}{A_{ref}} \tag{21}$$

Tee Nut Screw Connection Drag Coeffcient

$$C_{D(tn)} = 0.42\frac{A_{tn}C_{pT}}{A_{ref}} \tag{22}$$

Total Parasitic Drag Coefficient

$$C_{D(p)} = C_{D(r)} + C_{D(vh)} + C_{D(sp)} + C_{D(s)} \tag{23}$$

VIII. Compression Correction

Subscript "i" denotes type of drag

$$C_i' = \frac{C_i}{\sqrt{1 - M_a^2}} \tag{24}$$

IX. Shear Pins

Force to Shear a Single Shear Screw

$$F_{separate} = \frac{\pi D^2 \tau}{4} \tag{25}$$

Force of Black Powder to Cause Separation

$$F_{separate} = \frac{\pi D^2 P}{4} \tag{26}$$

Number of Shear Pins

$$N = \frac{F_{separate}}{F_{shear}} \tag{27}$$

Factor of Safety

$$n = \frac{F_{separate}}{F_{shear}N} \tag{28}$$

X. Kinematic Equations

$$F_{xn} = T_n cos(\theta_{n-1}) - D_n cos(\theta_{n-1}) - N_n sin(\theta_{n-1}) \tag{29}$$

$$F_{yn} = T_n sin(\theta_{n-1}) - m_n g - D_n sin(\theta_{n-1}) - N_n cos(\theta_{n-1}) \tag{30}$$

XI. Dynamic Equations

Subscript "i" denotes direction x or y

$$a_{in} = \frac{F_{in}}{m_{in}} \tag{31}$$

$$v_{in} = v_{in-1} + a_{in}\Delta t \tag{32}$$

$$r_{in} = r_{in-1} + v_{in}\Delta t \tag{33}$$

XII. Atmospheric Model

Pressure Change With Altitude

$$P_n = P_b\left(\frac{T_b}{T_b + L_b(r_{yn-1} - r_0)}\right)^{\frac{g_0 M}{R_U L_b}} \tag{34}$$

Air Density Change With Altitude

$$\rho_n = \rho_b\left(\frac{T_b}{T_b + L_b(r_{yn-1} - r_0)}\right)^{(1+\frac{g_0 M}{R_U L_b})} \tag{35}$$

Air Temperature Change with Altitude

$$T_n = T_b + L_b r_{yn-1} \tag{36}$$

Sutherland's Formula for Air Dynamic (Absolute) Viscosity Change with Temperature

$$\mu_n = 0.1456^{-5}\frac{\sqrt{T_n}}{1+\frac{110}{T_n}} \tag{37}$$

Speed of Sound Change with Temperature

$$a_n = \sqrt{\gamma R T_n} \tag{38}$$

XIII. Parachute

Descent Velocity

$$V = \sqrt{\frac{2W}{C_d r A}} \tag{39}$$

Parachute Surface Area

$$S = \frac{2gm}{rC_d V^2} \tag{40}$$

Parachute Diameter

$$D = \sqrt{\frac{4S}{\pi}} \tag{41}$$

XIV. Static Pressure Port Calculation

$$D = ID\left(\sqrt{\frac{\frac{\pi(\frac{1}{4}in)^2}{4}}{100in^2} * \frac{L}{N_{holes}}}\right) \tag{42}$$

XV. Miscellaneous

Mass of Black Powder Needed to Deploy Parachute

$$m_{bp} = \frac{\pi LPD}{4R_{bp}T_{combust}} \tag{43}$$

Mass of Fuel During Flight

$$m_n = m_i - m_{prop}\frac{t_n}{t_b} \tag{44}$$

$$\eta_{airfoil} = \frac{C_{D(airfoiled\cdot rb)}}{C_{D(cylindrical\cdot rb)}} \tag{45}$$

XVI. Shear Screw Sample Calculations

$$Force = \frac{\pi D^2 \tau}{4} = \frac{\pi(0.0641)^2(9430)}{4} = 32.27lb_f$$

$$Force = \frac{\pi D^2 P}{4} = \frac{\pi(6in)^2(8psi))}{4} = 226.19lb_f$$

$$N = \frac{226.19lb_f}{32.27lb_f} = 7.01$$

$$n = \frac{226.19lb_f}{(32.27)(6)} = 1.17$$

XVII. Payload Bay Sample Calculations

Bottom Disk Attached to Main Body

$$F = Ma = (4Kg + 0.184Kg)\left(23 * 9.81\,{}^{m}/_{s^2}\right) = 944.04N$$

$$Q = \frac{bh}{4} * \frac{h}{4} = \frac{0.4788m * 0.0127m}{4} * \frac{0.0127m}{4} = 9.653 * 10^{-6}m^3$$

$$I = \frac{bh^3}{12} = \frac{0.4788m * 0.0127^3m}{12} = 8.1 * 10^{-8}m^4$$

$$t = 0.0127m$$
$$\tau = \frac{QF}{It} = \frac{9.653 * 10^{-6}m^3 * 944.04N}{8.1 * 10^{-8}m^4 * 0.0127m} = 8.86MPa$$
$$Epoxy\ Shear\ Strength = 26.2MPa$$
$$n = \frac{26.2MPa}{8.86MPa} = 2.96$$

Bottom Disk Strength

$$F = 23\left(9.81\,{}^{m}/_{s^2}\right)4Kg = 902.59N$$
$$\tau = \frac{QF}{It} = \frac{9.653 * 10^{-6}m^3 * 902.59N}{8.1 * 10^{-8}m^4 * 0.0254m} = 4.235MPa$$
$$Shear\ Strength\ of\ Plywood = 6.2MPa$$
$$n = \frac{6.2MPa}{4.235MPa} = 1.42$$

Shear Stress in Nose Cone Bolts

Worst Case Scenario: Entire Nose cone and payload mass acting on the bolts

$$F = Ma = 6.67Kg * 23\left(9.81\,{}^{m}/_{s^2}\right) = 1504.86N$$
$$\tau_b = \frac{4F}{\pi d^2} = \frac{4 * 1504.86N}{\pi * 6.4^2 mm} = 46.778MPa$$
$$\tau_b\ per\ bolt = \frac{46.778MPa}{4} = 11.695.MPa$$
$$Ultimate\ Shear\ Strength = 150MPa$$
$$n = \frac{150MPa}{11.695MPa} = 12.9$$

XVIII. Fourier Number Analysis

Nusselt Number

$$Nu = (0.037Re^{0.8} - 871)Pr^{\frac{1}{3}} \quad (46)$$

Nusselt Number

$$Nu = \frac{hL}{k} \quad (47)$$

Fourier Number

$$\tau = \frac{\alpha t}{R^2} \quad (48)$$

Thermal Diffusivity

$$\alpha = \frac{k}{\rho C_{p1}} \quad (49)$$

APPENDIX H: MATLAB TRAJECTORY MODEL

I. Rocket Master Code

```
clear, clc, close all

%% Select a Motor (Based on Excel Sheet)
motorSelection = 14;

%%
%   ////////////////////////////////////////////////////
%   /////////////// IMPORT DATA ////////////////////////
%   ////////////////////////////////////////////////////

components = xlsread('RocketDimensions.xlsx','Components');
finGeometry = xlsread('RocketDimensions.xlsx','FinGeometry');
motorSpecs = xlsread('RocketDimensions.xlsx','MotorSpecs');
inputs = xlsread('RocketDimensions.xlsx','Inputs');
parasiticParameters = xlsread('Rocketdimensions.xlsx','ParasiticParameters');
boundaryConditions = xlsread('Rocketdimensions.xlsx','Inputs');

%%
%   ////////////////////////////////////////////////////
%   /////////////// INITIALIZATION /////////////////////
%   ////////////////////////////////////////////////////

% Technical Parameters
timeStep = 0.1;
Memory_Allocation = 10000;
n = 1;

% Memory Preallocations
t = zeros(1, Memory_Allocation);
thrust = zeros(1, Memory_Allocation);
mass = zeros(1, Memory_Allocation);
theta = zeros(1, Memory_Allocation);
normalForce = zeros(1, Memory_Allocation);
dragForce = zeros(1, Memory_Allocation);
x_force = zeros(1, Memory_Allocation);
y_force = zeros(1, Memory_Allocation);
x_acceleration = zeros(1, Memory_Allocation);
y_acceleration = zeros(1, Memory_Allocation);
resultantAcceleration = zeros(1, Memory_Allocation);
x_velocity = zeros(1, Memory_Allocation);
y_velocity = zeros(1, Memory_Allocation);
resultantVelocity = zeros(1, Memory_Allocation);
x_position = zeros(1, Memory_Allocation);
y_position = zeros(1, Memory_Allocation);
x_distance = zeros(1, Memory_Allocation);
y_distance = zeros(1, Memory_Allocation);
totalDistance = zeros(1, Memory_Allocation);

% Format
% figure('units','normalized','outerposition',[0 0 1 1])
format short g
```

```
%%
%   ////////////////////////////////////////////////
%   /////////////// DIMENSIONS /////////////////////
%   ////////////////////////////////////////////////

% Nose
ln = components(1,2);
dn = components(1,3);
% syms x_nose
% theta1 = acos(1 - 2*x_nose/ln);
% y_nose = ((dn/2)/sqrt(pi))*sqrt(theta1 - 1/2*sin(2*theta1));
% A_func = int(2*pi*y_nose,0,ln);
% A_nose_surface = vpa(A_func,6);
A_nose_surface = 0.289081;

% Body
lb = components(3,2) + components(4,2);
lc = 0;
lTR = lb + ln;
db = components(3,3);
du = db;
dd = db;
Ap_n = ln*dn/2;
Ap_b = lb*db;
Acs = (db^2)*pi/4;

% Fin Dimensions
lt = finGeometry(1);
ls = finGeometry(2);
lr = finGeometry(3);
lw = finGeometry(4);
lm = finGeometry(5);
lTS = finGeometry(6);
df = finGeometry(7);
wf = finGeometry(8);
Xf = finGeometry(9);
tf = finGeometry(10);
N = finGeometry(11);
Ae_f = finGeometry(12);
Ap_f = finGeometry(13);

% Exposed Holes, Rail Buttons, Screws/Rivets, Shear Pins, & Surface Roughness
Height
N_hole = parasiticParameters(1);
N_rail_button = parasiticParameters(2);
A_rail_button = parasiticParameters(3);
N_shear_pin = parasiticParameters(4);
A_shear_pin = parasiticParameters(5);
N_screw = parasiticParameters(6);
Rs = parasiticParameters(7);
gamma = 1.4;
R = 287;

%%
%   ////////////////////////////////////////////////
```

```
%   /////////////// PARAMETERS ////////////////////////
%   ////////////////////////////////////////////////////

% User Inputs and Initial Values
groundTemp = inputs(1,1);
groundPressure = inputs(1,2);
y_position(1) = inputs(1,3);
lapseRate = inputs(1,4);
surfaceRoughness = inputs(1,5)/(1e6);
launchRodLength = inputs(1,6);
theta(1) = 90 - inputs(1,7);

airTemp(1) = groundTemp;
airPressure(1) = groundPressure;
airDensity(1) = groundPressure/(R*groundTemp);
speedSound(1) = sqrt(R*gamma*groundTemp);
dynamicViscosity(1) = 0.1456E-5*(sqrt(groundTemp)/(1 + 110/groundTemp));

x_velocity(1) = 0;
y_velocity(1) = 0;
x_position(1) = 0;

mass(1) = sum(components(:,1));
initialFuel = components(20,1);
centreMass(1) = calculatecentremass(components,initialFuel,0,mass(1));
%%
%   ////////////////////////////////////////////////////
%   ////////////// ROCKET PHYSICS ////////////////////////
%   ////////////////////////////////////////////////////

%% CENTER OF PRESSURE
centrePressure = calculatecentrepressure(df,ls,N,dn,lm,lr,lt,Xf,ln);

while y_position(n) >= y_position(1)

    %% TIME STEP
    n = n+1;
    t(n)= (n-1)*timeStep;

    %% ATMOSPHERIC MODEL

[airTemp(n),airDensity(n),airPressure(n),dynamicViscosity(n),soundSpeed(n),g(
n)] = ...
        atmosphericmodel(y_position(n-
1),groundTemp,lapseRate,gamma,R,groundPressure,y_position(1));

    % Mach Number Calculation
    machNo(n) = resultantVelocity(n-1)/speedSound;


    %% LAUNCH PHASES
    [thrust(n),mass(n),fuelBurned(n)] =
launchphases(motorSpecs,motorSelection,mass(1),t(n));
```

```
    %% CENTER OF MASS
    centreMass(n) =
calculatecentremass(components,initialFuel,fuelBurned(n),mass(n));

    %% COEFFICIENT OF DRAG
    % Coefficients of Drag

[coeff_skinDrag(n),coeff_baseDrag(n),coeff_finDrag(n),coeff_interferenceDrag(
n),coeff_parasitic(n)] = ...

coefficientdrag(airDensity(n),dynamicViscosity(n),lTR,ln,lb,lc,lm,db,dd,df,tf
,...
        resultantVelocity(n-
1),gamma,machNo(n),Ap_f,Ae_f,Acs,A_shear_pin,A_rail_button,N,N_hole,...
        N_rail_button,N_shear_pin,N_screw,surfaceRoughness);

    % Compressibility Correction

[correctedCoeff_skinDrag(n),correctedCoeff_baseDrag(n),correctedCoeff_finDrag
(n),correctedCoeff_interferenceDrag(n),correctedCoeff_parasiticDrag(n)] = ...

compressibilitycorrection(coeff_skinDrag(n),coeff_baseDrag(n),coeff_finDrag(n
),coeff_interferenceDrag(n),machNo(n),coeff_parasitic(n));

    % Total Drag Coefficient
    correctedCoeff_totalDrag(n) =
correctedCoeff_skinDrag(n)+correctedCoeff_baseDrag(n)+ ...

correctedCoeff_finDrag(n)+correctedCoeff_interferenceDrag(n)+correctedCoeff_p
arasiticDrag(n);

    %% KINEMATICS
       %% KINEMATICS
    [x_force(n),y_force(n)] = calculateforce(totalDistance(n-
1),boundaryConditions(5),mass(n),theta(n-1),theta(1), ...
        correctedCoeff_totalDrag(n),airDensity(n),Acs,resultantVelocity(n-
1),thrust(n),t(n));
    %% DYNAMICS
    % Acceleration
    x_acceleration(n)= x_force(n)/mass(n);
    y_acceleration(n)= y_force(n)/mass(n);
    resultantAcceleration(n) = sqrt(x_acceleration(n)^2 +
y_acceleration(n)^2);

    % Velocity
    x_velocity(n)= x_velocity(n-1)+x_acceleration(n)*timeStep;
    y_velocity(n)= y_velocity(n-1)+y_acceleration(n)*timeStep;
    resultantVelocity(n) = sqrt(x_velocity(n)^2 + y_velocity(n)^2);

    % Position
    x_position(n)= x_position(n-1)+x_velocity(n)*timeStep;
    y_position(n)= y_position(n-1)+y_velocity(n)*timeStep;
    alt(n) = y_position(n) - y_position(1);

    % Distance
```

```
    x_distance(n) = x_distance(n-1)+abs(x_velocity(n)*timeStep);
    y_distance(n) = y_distance(n-1)+abs(y_velocity(n)*timeStep);
    totalDistance(n) = (x_distance(n)^2+y_distance(n)^2)^(1/2);

    % Angle With Respect to Y-Axis
    theta(n)= atand(y_velocity(n)/x_velocity(n));

end

%%
%   ////////////////////////////////////////////////
%   ////////////// IMPORTANT RESULT ////////////////
%   ////////////////////////////////////////////////

Apogee = max(alt)
Max_Velocity = max(resultantVelocity)
Max_Acceleration = max(resultantAcceleration);
CG_1 = centreMass(1)
CG_2 = min(centreMass)
CP = centrePressure
Stability = (CP - CG_1)/db
Total_Mass = mass(1)
tempmin=min(airTemp)
tempmax=max(airTemp)
tempavg=(tempmax+tempmin)/2
tempC=tempavg-273.15
```

II. Calculate Force Function

```
function [Fx,Fy] =
calculateforce(Distance,launchRodLength,Mass,Theta,launchAngle,Cd_R,airDensit
y,Acs,resultantVelocity,Thrust,t)

    % Constants
    g = 9.81;

    % Parachute Shit
    t_drogue = 27.25;
    t_main = 100;
    Cd_drogue = 0.75;
    Cd_main = 2.59;
    A_drogue = 0.466 ;      % Area here
    A_main = 1;         % Area here

    % Normal Force
    if Distance <= launchRodLength
        Normal = Mass*g*cosd(launchAngle);
    else
    % Normal(n) = 0.5*Cn(n)*Rho*A*(Vx(n-1)^2+Vy(n-1)^2);
        Normal = 0;
    end

    if t < t_drogue
```

```
    coefficient_ofDrag = Cd_R;
        respective_Area = Acs;

    elseif t >= t_drogue && t< t_main
    coefficient_ofDrag = Cd_drogue;
        respective_Area = A_drogue;

    elseif t >= t_main
    coefficient_ofDrag = Cd_main;
        respective_Area = A_main;

    end


    % Drag Force
    Drag=
0.5*coefficient_ofDrag*airDensity*respective_Area*(resultantVelocity^2);

    % Sum of Forces
    Fx = Thrust*cosd(Theta)-Drag*cosd(Theta)...
        -Normal*sind(Theta);
    Fy = Thrust*sind(Theta)-(Mass*g)-...
        Drag*sind(Theta)+Normal*cosd(Theta);
```

III. Launch Phases Function

```
function [Thrust,Mass,fuelBurned] =
launchphases(motorSpecs,motorSelection,totalMass,t)
% The different phases the rocket will go through during flight, from
% initial launch, to apogee, and recovery.

% Burn Phase
    if t <= motorSpecs(motorSelection,2)
        Thrust = motorSpecs(motorSelection,1)/motorSpecs(motorSelection,2);
        fuelBurned =
motorSpecs(motorSelection,4)*t/motorSpecs(motorSelection,2);

% Coast Phase
    elseif t >= motorSpecs(motorSelection,2)
        Thrust = 0;
        fuelBurned = motorSpecs(motorSelection,4);
    end

        Mass = totalMass - fuelBurned;

end
```

IV. Centre of Pressure Function

```
function [Xcpr_R] = calculatecentrepressure(df,ls,N,dn,lm,lr,lt,Xf,ln)
% Centre of pressure calculation for the rocket, based only on the
```

```
% outer geometry. This only includes nose and fins, and ignores body lift.


    % Parts Stability Derivative
    Kfb = 1 + (df/2)/(ls+(df/2));
    Cna_f = Kfb*(4*N*(ls/dn)^2)/(1+ sqrt(1+(2*lm/(lr+lt))^2));

    Cna_P = [
        2
        Cna_f
    ];

    % Parts Centre of Pressure
    Xcpr_f = Xf + (lm*(lr+2*lt))/(3*(lr+lt)) + (1/6)*(lr+lt-(lr*lt/(lr+lt)));

    Xcpr_P = [
        (0.5)*ln
        Xcpr_f
    ];

    % Rocket Centre of Pressure
    Cna_R = sum(Cna_P);
    Xcpr_R = sum(Cna_P(:,1).*Xcpr_P(:,1))/Cna_R;

end
```

V. Centre of Mass Function

```
function [centreMass] =
calculatecentremass(components,initialFuel,fuelBurned,totMass)
% Centre of mass calculation for the rocket, based on the given geometries
% inputted into the RocketDimensions excel sheet. Calculates based on
% inner component lengths and weights, and is all relative to the nose tip.

components(20,1) = initialFuel - fuelBurned;
centreMass = sum(components(:,1).*components(:,4))/totMass;

end
```

VI. Coefficient of Drag Function

```
function [Cd_fb,Cd_b,Cd_f,Cd_i,Cd_parasitic] =
coefficientdrag(airDensity,dynamicViscosity,lTR,ln,lb,lc,lm,db,dd,df,tf,resul
tantVelocity,gamma,machNo,Ap_f,Ae_f,Acs,A_shear_pin,A_rail_button,N,N_hole,N_
rail_button,N_shear_pin,N_screw,Rs)
% Drag cofficient calculation. The drags involved will be skin drag (Cd_fb),
% base drag (Cd_b), fin drag (Cd_f), and interference drag (Cd_i).
%
gamma,machNo,Ap_f,Ae_f,Acs,A_shear_pin,A_rail_button,N,N_hole,N_rail_button,N
_shear_pin,N_screw,Rs
%% Flow Properties
```

```
    Re_b = (airDensity*resultantVelocity*lTR)/dynamicViscosity;
    Re_f = (airDensity*resultantVelocity*lm)/dynamicViscosity;
    ReC_b = 51*(Rs/lTR)^(-1.039);
    ReC_f = 51*(Rs/lm)^(-1.039);

%% Skin Friction Coefficient

%   Body
    if Re_b <= 10E4
       Cf_fb = 1.48E-2;

    elseif Re_b > 10E4 && Re_b <= ReC_b
       Cf_fb = 1/((1.5*log(Re_b)-5.6))^2;

    elseif Re_b > ReC_b
       Cf_fb = 0.032*(Rs/lTR)^0.2;

    end

%   Fin
    if Re_f <= 10E4
       Cf_f = 1.48E-2;

    elseif Re_f > 10E4 && Re_f <= ReC_f
       Cf_f = 1/((1.5*log(Re_f)-5.6)^2);

    elseif Re_f > ReC_f
       Cf_f = 0.032*(Rs/lm)^0.2;

    end

%% Skin Drag Coefficient
    B_fb = ReC_b*(0.074/Re_b^(1/5) - 1.328/sqrt(Re_b));
    Cd_fb =  (1 + 60/(lTR/db)^3 + 0.0025*(lb/db))*...
                (2.7*(ln/db) + 4*(lb/db) + 2*(1 - (dd/db))*(lc/db))*Cf_fb;

%     A_body_wet = A_nose_surface + lb*(pi*db) + N*Ae_f;
%     Cf_surface_rough_total = Cf_surface*(((1 + 2*lTR/db)*A_body_wet + (1 +
2*tf/lm)*2*Ae_f)/Acs);

%% Base Drag Coefficient
    Cd_b = 0.029*(dd/db)^3/sqrt(Cd_fb);

%% Fin Drag Coefficient
    B_ff = ReC_f*(0.074/Re_f^(1/5) - 1.328/sqrt(Re_f));
    Cd_f = 2*Cf_f*(1 + 2*(tf/lm))*((4*N*Ap_f)/(pi*df^2));

%% Interference Drag Coefficient
    Cd_i = 2*Cf_f*(1 + 2*(tf/lm))*((4*N)*(Ap_f - Ae_f)/(pi*df^2));

%% Parasitic Drag Coefficient
```

```
    % Apogee Components Airfoiled Rail Button
    if machNo ==0
        P_ratio = 0;
        C_pt = 0;
    else
        P_ratio = (1+machNo^2*(gamma-1)/2)^(gamma/(gamma-1));
        C_pt = (P_ratio - 1)*(2/(gamma*machNo^2));
    end

    Rail_Button_Efficiency = 0.3/0.57;
    Cd_rail_button = 0.8*Rail_Button_Efficiency*A_rail_button*C_pt/Acs;

    % Vent Hole
    Cd_hole = 0.0041*(pi/4*0.003^2)*C_pt/Acs;

    % Shear Pin (Round rivet head)
    Cd_shear_pin = 0.32*A_shear_pin*C_pt/Acs;

    % Screw Head
    Cd_screw = 0.42*(pi/4*0.01905^2)*C_pt/Acs;

    % Total Parasitic Drag
    Cd_parasitic = N_hole*Cd_hole + N_rail_button*Cd_rail_button +
N_shear_pin*Cd_shear_pin + N_screw*Cd_screw;
%    Cd_parasitic = 0;

end
```

VII. Compressibility Correction Function

```
function [Cd_fbi,Cd_bi,Cd_fi,Cd_ii,Cd_parasitici] =
compressibilitycorrection(coeff_skinDrag,coeff_baseDrag,coeff_finDrag,coeff_i
nterferenceDrag, machNo,coeff_parasitic)
% Compressibility correction calculation for subsonic (Mach < 1) and
% supersonic (Mach > 1) regime, using the Prandtl-Glauert rule.

    % Subsonic
    if machNo <= 1 && machNo >= 0
        Cd_fbi = coeff_skinDrag/sqrt(1-machNo^2);
        Cd_bi = coeff_baseDrag/sqrt(1-machNo^2);
        Cd_fi = coeff_finDrag/sqrt(1-machNo^2);
        Cd_ii = coeff_interferenceDrag/sqrt(1-machNo^2);
        Cd_parasitici = coeff_parasitic/sqrt(1 - machNo^2);

    % Supersonic
    elseif machNo > 1
        Cd_fbi = coeff_skinDrag/sqrt(machNo^2-1);
        Cd_bi = coeff_baseDrag/sqrt(machNo^2-1);
        Cd_fi = coeff_finDrag/sqrt(machNo^2-1);
        Cd_ii = coeff_interferenceDrag/sqrt(machNo^2-1);
        Cd_parasitici = coeff_parasitic/sqrt(machNo^2-1);

    end
```

```
end
```

VIII. Atmospheric Model Function

```
function [airTemp,airDensity,airPressure,dynamicViscosity,soundSpeed,g] =
atmosphericmodel(yPosition,groundTemp,lapseRate,gamma,R,groundPressure,initia
lPosition)

    % Constants
    Mo = 0.0289644;
    Ru = 8.3142;
    g_0 = 9.79143;
    r_earth = 6371000;
    % Gravity
    g = g_0*(r_earth/(r_earth + yPosition))^2;

    % Air Temperature
    airTemp = groundTemp + lapseRate*(yPosition - initialPosition);

    % Air Density
    airPressure = groundPressure*(groundTemp/(groundTemp +
lapseRate*(yPosition - initialPosition)))^((g*Mo)/(Ru*lapseRate));

    % Air Density
    airDensity = airPressure/(R*airTemp);

    % Dynamic Viscosity (Sutherland's formula)
    dynamicViscosity = 0.1456E-5*(sqrt(airTemp)/(1 + 110/airTemp));

    % Local Speed of Sound
    soundSpeed = sqrt(gamma*R*airTemp);

end
```